FLUX CALIBRATIONS FROM NEARBY ECLIPSING BINARIES AND SINGLE STARS

R. E. Wilson[1], W. Van Hamme[2], and Dirk Terrell[3]
[1] Astronomy Department, University of Florida, Gainesville, FL 32611, USA
[2] Department of Physics, Florida International University, Miami, FL 33199, USA; vanhamme@fiu.edu
[3] Department of Space Studies, Southwest Research Institute, Boulder, CO 80302, USA; terrell@boulder.swri.edu

ABSTRACT

Eclipsing binaries (EBs) measure distance without need or use for nearby similar objects, with many applications over recent decades. EBs are now considered the most reliable and accurate distance indicators for the very important lower rungs in the cosmic distance ladder, within the Local Group of Galaxies. Among several EB distance algorithms, direct comparison of observed and theoretical fluxes is particularly straightforward, although it requires absolute flux calibrations for which only a modest number of publications exist. Here, we measure *UBV RI* and *uvby* flux calibrations and calibration ratios from astronomical objects in ways not previously tried, specifically for EBs, single stars within 80 pc, and the Sun. All of the single stars are below about 6500 K temperature. Interstellar extinction is avoided by a restriction to nearby targets. Some photometric band calibrations in the literature are accurate enough for very good EB distance determinations if star temperatures are accurately known, especially considering that estimated distance has only a square-root dependence on calibration constant, but accurate band-to-band calibration *ratios* are keys to the combined temperature–distance problem. Band-independent canceling factors (star radii and distances) allow calibration ratio measurement with enhanced accuracy, compared to individual band calibrations. A physical EB model with embedded stellar atmosphere emission optimally matches theory to observations for the binaries. Single star candidates are identified as reliably single if their radial velocity variations are below 100 m s^{-1}. For the most part, we find good agreement with some of the previous calibrations and the ratios are improved.

Key words: binaries: close – binaries: eclipsing – binaries: spectroscopic – stars: distances

Online-only material: machine-readable tables

1. ECLIPSING BINARY DISTANCE ACCURACY

Eclipsing binaries (EBs) allow accurate distance measurement to objects as remote as the relevant observations can be made, which today is within the Local Group of Galaxies (Bonanos et al. 2006; Vilardell et al. 2010). Numerous papers over the past decade have demonstrated that EBs realistically provide distances as accurately as does trigonometric parallax and for vastly more remote objects. The central concept is that all dimensional and radiative quantities needed for an accurate distance estimate are measured quantitatively for a well-observed and well-conditioned EB. Relative dimensions come from light curves, the dimensional scale comes from radial velocities (RVs), and radiative emission comes from temperatures that can be estimated in several ways. Nearby similar examples are not needed and actually play no role whatever in EB distance estimation, unlike standard candles such as Cepheids and supernovae. Standard candles (one of the few options for distances beyond the Local Group) do need comparatively nearby reference objects, whose distances can be inferred if they are in the same composite systems (say galaxies or star clusters) as EBs, so EBs can be involved in setting truly cosmic distance scales.[4]

Therefore, continued optimization of EB distance measurement is important to the wider distance problem. Simulations show that, given observations of typical good accuracy, EB distances are good to a few percent or better in the ideal case that the

"calibrative" information (model stellar atmospheres, transformations to standard photometric systems, and flux calibrations) is free of systematic error. Surely, it would be desirable to know distances everywhere in the Local Group to a few percent, especially if they are essentially model independent, as are EB distances (i.e., based entirely on well-established physics and geometry). Accordingly, the calibrative issues need to be addressed one by one. In this paper, we address flux calibrations with emphasis on their band-to-band ratios.

The basic ideas of EB distance measurement go back at least to Russell (1948) and perhaps further, with many references in Kruszewski & Semeniuk (1999), but relatively recent remarks (Paczynski 1997) alerted the community and led to many EB-based distance applications, e.g., Guinan et al. (1998), Ostrov & Lapasset (2003), Clausen et al. (2003), Harries et al. (2003), Wilson (2008), and Wilson & Van Hamme (2009). In another development, required calibrations are now more accurate than in decades past. Several variations on the fundamental EB-based distance concept are in use, and each operates with a specific kind of calibration.

1.1. Capsule Summary of Direct Distance Estimation

The procedure of interest here is that of Wilson (2007, 2008), called Direct Distance Estimation (DDE). DDE generates model fluxes in standard physical units (specifically erg s^{-1} cm^{-3}), with full incorporation of all ordinary close binary effects. Given a few reliable calibration numbers, DDE can lead to accurate and easy distance estimates of known uncertainty. They are accurate because spherical star approximations are entirely avoided, easy because distance is an ordinary solution parameter, and of known uncertainty because they are accompanied by standard errors. The DDE algorithm has been inserted into the 2010

---

[4] An important literature on luminosity measurement for Cepheids based on interferometry has developed, mostly over the last decade (e.g., Welch 1994; Kervella et al. 2004; Macri 2005; Barnes et al. 2005; Storm et al. 2005; Gieren et al. 2005; Di Benedetto 2005, 2008; Fouque et al. 2007; Eisner et al. 2007; Davis et al. 2009; Barnes 2009). EB and interferometric Cepheid calibrations can serve as mutual checks.

version[5] of the Wilson–Devinney (hereafter WD) EB light curve and RV analysis program (Wilson & Devinney [1971]; Wilson [1979], [1990], [2008]). The model fluxes are compared with absolute observed fluxes computed from magnitudes in standard photometric systems such as Johnson *UBV RIJK* or Strömgren *uvby*. A DDE advantage compared to other variants of EB distance estimation is that it works as well for over-contact (OC) and near-contact systems as for well-detached EBs, which is important because most viable targets are not well detached. DDE requires band-dependent magnitude to flux calibrations, each expressed as observable flux from a zero magnitude star ($C_{\rm band}$). Accurate $C_{\rm band}$ ratios such as C_B/C_V and C_U/C_B impress coherence on the set of all band calibrations and thereby on overall band-to-band results from absolute EB solutions. However, their primary value is in producing good temperature estimates for both EB components by correctly accessing information in multiple bands. Distances, which are correlated with temperatures, are correspondingly also improved.

A brief summary of EB distance estimation via the DDE algorithm will clarify its use for flux calibration measurements, which are basically inverted DDE applications ($C_{\rm band}$ from distance d rather than d from $C_{\rm band}$). In a given standard photometric band, one has $d = d$(EB parameters, $C_{\rm band}$), where some of the EB parameters are derivable mainly from light curves, some mainly from RVs, some from spectral classification or spectral modeling, and perhaps others from miscellaneous further information. DDE inputs a mix of observed light curves (perhaps multi-band) and RV curves, a $C_{\rm band}$ for each light curve, and adopted parameters related to phenomena such as gravity brightening and the reflection effect. It then converts the light curve observations to absolute fluxes via the $C_{\rm band}$'s, compares the fluxes with model fluxes computed from the EB parameters, and eventually arrives at a solution for designated parameters, including d, by the least-squares criterion. Bandpass emission is computed locally on each star (Van Hamme [1993]; Van Hamme & Wilson [2003]) from stellar atmosphere results (Kurucz [1993]) that are embedded within the analysis program. A binary's morphological type is not an issue because parameter d is intrinsic to the model regardless of type, and the distance logic rigorously applies all the usual aspect effects. Note that other variations (i.e., non-DDE) on EB distance estimation assume spherical stars in a separate distance finding step and accordingly most of their applications have avoided binaries that are not well detached. Such rejections of good targets are unnecessary in DDE.

1.2. Importance of Band-to-Band Flux Calibration Ratios

$C_{\rm band}$'s have previously been found by numerical integration of absolute spectral energy distributions (SEDs) over photometric response curves (Johnson [1965a], [1966]; Tapia et al. [1973]; Bessell [1979]; Heber et al. [1984]; Helt et al. [1991]; Fabregat & Reig [1996]; Gray [1998]; Cohen et al. [2003]), and several ways to evaluate such calibrations are explained in those papers. Mutual agreement among some of the published $C_{\rm band}$ sets and agreement between DDE and *Hipparcos* parallax distances (Wilson [2008]; Wilson & Van Hamme [2009]) demonstrate that individual $C_{\rm band}$'s are accurate enough for good distance estimates where a temperature for one of the components is known. Wilson ([2008]) distinguished between solutions for temperature[6] of one

EB component and both components ($1T$ and $2T$ solutions) and noted that $2T$ temperature determinations require light curves in two bands and are sensitive to $C_{\rm band}$ ratios, although derived temperatures are unaffected if the $C_{\rm band}$'s are changed together so as to keep a fixed ratio (Section [2.1]). Accordingly, accurate $C_{\rm band}$ ratios are crucial to success of $2T$ solutions, which offer an alternative to spectroscopic temperatures for favorable examples. Temperatures based on spectral classification are subjective and almost always refer to an unknown orbital phase, as observation times of the relevant spectra are seldom reported.[7] Other problems with spectroscopic temperatures are that spectral types are discontinuous and coarsely spaced and that separation of T_1 from T_2 in binaries may be difficult spectroscopically.

1.3. Effective Utilization of Flux Calibrations to Find Eclipsing Binary Distances

Taken together, these points about prior establishment of $C_{\rm band}$ *ratios* mean that instead of N unrelated calibrations for N bands, accurate $C_{\rm band}$ determination for one band can set good calibrations for other bands if the ratios are known. Given correct temperatures, distance depends only weakly on $C_{\rm band}$ (by a factor of $\sqrt{1/C_{\rm band}}$), but a wrong $C_{\rm band}$ ratio mimics a wrong (band-to-band) flux ratio so as to give wrong temperatures in $2T$ solutions, while accurate temperatures are needed for accurate distance. Accordingly, accurate $C_{\rm band}$ ratios are the keys to temperature estimation without spectra[8] with full utilization of light curve temperature information.

After refinement of the $C_{\rm band}$ ratios, distances can be found routinely in subsequent $2T$ solutions without knowledge of spectral types if interstellar extinction is measurable or negligible. Overall, a typical 1σ uncertainty in T from spectral type is of the order of several percent. An alternative for temperature estimates is color index, but color index calibrated for single stars may not apply reliably to unresolved binaries, most of which are two-temperature sources. A further difficulty requiring proper inversion of binary effects is that color indices saturate (approach fixed values) for very hot stars, thereby losing much of their usefulness as temperature indicators. Although spectral type will sometimes be the best option for temperature estimation and ordinary color index may be satisfactory for some EBs, simultaneous light-velocity EB solutions in two bands can be a third way. Such two-band solutions effectively rely on color index to set temperatures, but with thorough modeling of its variation with phase due to EB effects, two-temperature effects, and their interaction. The subjectivity of spectral classification is then bypassed.

2. FLUX CALIBRATIONS FROM ECLIPSING BINARIES AND SINGLE STARS

Confidence in calibrations increases when several classes of objects yield accordant results. The calibrations found in this paper have in common that all refer to the photometric response functions adopted in the WD program but, as explained below, specifics of their measurement differ for EBs, single stars, and the particular case of the Sun. A given star system has only one real distance so, if all $C_{\rm band}$'s for a given object are found

---

[5] Public program release via FTP download is expected for late 2010.

[6] The actual solution parameter is a mean effective temperature over the surface, not accounting for re-radiated energy, and weighted by local bolometric flux.

[7] One might think that time is routinely published for nearly all observations but often the time goes entirely unreported—even the *year*. The importance of an observation time may become apparent only long after publication.

[8] Unknown amounts of interstellar extinction can undermine T and d estimates, although our work in progress (Wilson & Van Hamme [2010]) suggests that extinction estimation from DDE solutions may be realistically possible in some cases.

together, percent C_{band} error due to distance error is the same for all bands and measured C_{band} ratios are therefore distance independent. This circumstance is important for an EB, where individually estimated C_{band}'s depend on the (inverse) square of the assumed distance.

The relative importance of various kinds of errors (stellar emission, photometric transformations, flux calibration constants, etc.) for EB distance measurement is difficult to assess. However, stellar atmosphere emission is probably correct within a few percent when averaged over a band while transformations by observers to standard photometric systems should also be accurate within a few percent, and better for uncomplicated objects. Fabregat & Reig (1996) list C_{band} uncertainties of 3%–4% that translate to distance errors of only 1.5%–2% because inferred distance scales (inversely) with the square root of observed flux, so flux calibrations would appear to be only minor contributors to overall uncertainties. However, the concern here is mainly with band-to-band calibration ratios, which enter the multi-band problem in a complicated way and can introduce larger distance and temperature errors if inaccurate, as explained in Section 2.1.

Single stars of definite brightness and temperature—if reliably known to be single—can supply useful C_{band}'s in their own way, as described in Section 2.2. The number of suitable single star targets greatly exceeds that of EBs, so averages from hundreds or even thousands of stars can produce rather accurate C_{band}'s and C_{band} ratios.

2.1. Eclipsing Binaries: Flux Calibration by Inversion of Direct Distance Estimation

DDE can find not only d as a function of C_{band} but can run inversely, estimating C_{band}'s where distance is known. If d is fixed in separate (say) B and V solutions, in accordance with a given EB having only one distance, the derived C_B/C_V ratio will be independent of d and should be accurate if the $B - V$ color index is accurate and interstellar extinction is negligible. The reason is that a C_{band} measure depends strictly on adopted d according to the inverse square law of flux dilution, such that any error due to d cancels exactly in the C_B/C_V ratio. This exact cancellation (with other parameters fixed) has been checked by DDE simulations. Temperature dependence remains, but ordinarily will go in the same sense in the two bands so as to be far less important in the ratio than in the individual C_{band}'s. Coherence is therefore improved in simultaneous solutions that measure calibrations in two or more bands. C_{band} ratios of thus enhanced accuracy lead to much improved $2T$ solutions, as confirmed by further simulations. In subsequent applications to measure distance, errors in C_{band} ratios are equivalent to flux ratio errors that correspond to temperature errors, while temperatures are correlated with distance, so accurate C_{band} ratios are crucial to reliability of temperature and distance.

2.2. Nearby Single Stars

Our single star C_{band} estimation scheme differs from calibrations in the previous literature so as to check earlier results independently, while following the essential information usage of DDE solutions. In other words, the plan is to have a consistent line of attack for EBs and single stars that does not simply repeat previous work. We operate with band-integrated absolute model stellar atmosphere fluxes to find C_{band}'s for individual stars and then average the C_{band}'s for many stars. Typical earlier work generates band-integrated fluxes over absolute *empirical*

SEDs, then averages the fluxes. Although our procedure works in combination with geometric and model stellar atmosphere parameters and therefore is less straightforward than the traditional one, it becomes absolute in its own way and thus gives new results.

Band calibration for a single spherical star is given in terms of apparent magnitude (m) and computed surface flux (f), in the absence of interstellar extinction, by

$$C_{band} = 10^{0.4m} f_{band} \left(\frac{R}{d} \right)^2. \tag{1}$$

R and d are the same for all bands so the R/d factor cancels exactly in band-to-band ratios. The radius and star mass ($\mathcal{M}$) also enter the computation through the effect of surface gravity, $g = G\mathcal{M}/R^2$, on theoretical stellar atmospheres, but only slightly since the computed SEDs depend mainly on T and only weakly on g. Taking the B, V ratio, for example, one finds

$$\frac{C_B}{C_V} = 10^{0.4(B-V)} \left(\frac{f_B(T, \log g, [M/H])}{f_V(T, \log g, [M/H])} \right), \tag{2}$$

where of course T, $\log g$, and chemical composition [M/H] are all band independent. Since distance cancels exactly in C_{band} ratios, the only reason to prefer nearby stars for the ratios is to be sure of negligible extinction.

The main selection requirement is that the stars be effectively single, as judged by having only the very small or undetectable velocity variations found in some exoplanet search targets. That is, they should not have companions of stellar mass (and luminosity), although they may have planets. The input data on T, $\log g$, [M/H], R, and d are taken from Tables 8 and 9 of the exoplanet paper by Valenti & Fischer (2005, hereafter VF) after removal of candidates with 1σ variations of more than 100 m s^{-1} according to Tables 1 and 2 of Nidever et al. (2002). All of our utilized single stars are within about 80 pc, as seen in Figure 13 of VF and therefore will have negligible, or at least unimportant, interstellar extinction. Any star with a double or variable star label or that appears in the Ninth Catalog of Spectroscopic Binary Orbits (Pourbaix et al. 2009) was rejected. Valenti & Fischer computed $R/R_\odot$ from $(L/L_\odot)^{1/2}/(T/T_\odot)^2$, where the L's are bolometric and based on distances from three parallax catalogs (mainly Perryman et al. 1997). We adopted the VF radii although, as a check, we computed the radii in another way—from V magnitudes and model stellar atmosphere emission in the V band, with revised HIP parallaxes by van Leeuwen (2007). We found R's that are almost the same as VF's. Actually the distance numbers, whether from 1997 HIP, 2007 HIP, or another source, are essentially irrelevant to single star C_{band} estimation. The reason is that simple geometric considerations require that R estimates, whether done in the VF way or in our way, are strictly proportional to d, so the calculated R/d's needed in Equation (1) are independent of input d. The ratio R/d will change from star to star due to other parameters but, except for very small $\log g$ effects, input distances are irrelevant for output C_{band}'s. Standard magnitude data are from three catalogs that are referenced in Table 1. This procedure yields calibration constants and calibration ratios for 462 stars in Strömgren $uvby$ (set 1), 310 in Johnson UBV (set 2), and 57 in Johnson $UBV RI$ (set 3). Mean values are in Table 1 and individual star results are in Table 2. Table 1 has two sets of C_{band} and C_{band} ratio columns, one for all accepted stars and one for the subset above $T = 5300$ K. The reason is that the corresponding figures (Figures 1–10) show that stars below

Table 1
$C_{\rm band}$'s and $C_{\rm band}$ Ratios for Single Stars

Quantity	N	Mean	σ_m	σ_m/Mean	N	Mean	σ_m	σ_m/Mean
		All Stars			Stars With $T_{\rm eff} > 5300$ K Only			
			Set 1, Strömgren *uvby*[a]					
C_u	462	1.1779	0.0037	0.0031	383	1.1740	0.0035	0.0030
C_v	462	0.8420	0.0016	0.0019	383	0.8356	0.0012	0.0015
C_b	462	0.58895	0.00046	0.00079	383	0.58834	0.00048	0.00081
C_y	462	0.37415	0.00016	0.00043	383	0.37428	0.00017	0.00047
C_u/C_v	462	1.3980	0.0025	0.0018	383	1.4040	0.0024	0.0017
C_u/C_b	462	1.9988	0.0051	0.0026	383	1.9947	0.0050	0.0025
C_u/C_y	462	3.1484	0.0099	0.0031	383	3.1372	0.0097	0.0031
C_v/C_b	462	1.4293	0.0020	0.0014	383	1.4201	0.0013	0.0009
C_v/C_y	462	2.2505	0.0043	0.0019	383	2.2327	0.0033	0.0015
C_b/C_y	462	1.5741	0.0011	0.00068	383	1.5720	0.0011	0.00070
			Set 2, Johnson *UBV*[b]					
C_U	310	0.4306	0.0020	0.0046	235	0.4236	0.0017	0.0040
C_B	310	0.6266	0.0012	0.0019	235	0.6225	0.0011	0.0018
C_V	310	0.36895	0.00036	0.00097	235	0.36883	0.00042	0.00114
C_U/C_B	310	0.6864	0.0021	0.0030	235	0.6801	0.0019	0.0027
C_U/C_V	310	1.1671	0.0051	0.0044	235	1.1485	0.0045	0.0039
C_B/C_V	310	1.6984	0.0027	0.0016	235	1.6877	0.0025	0.0015
			Set 3, Johnson *UBV RI*[c]					
C_U	49	0.4221	0.0044	0.0105	32	0.4167	0.0040	0.0095
C_B	50	0.6235	0.0029	0.0046	33	0.6202	0.0034	0.0055
C_V	57	0.36949	0.00084	0.0023	40	0.3691	0.0011	0.0030
C_R	57	0.17813	0.00085	0.0048	40	0.18026	0.00089	0.0049
C_I	55	0.08643	0.00058	0.0067	38	0.08785	0.00061	0.0069
C_U/C_B	49	0.6766	0.0047	0.0069	32	0.6721	0.0040	0.0060
C_U/C_V	49	1.142	0.012	0.010	32	1.1284	0.0096	0.0085
C_U/C_R	49	2.385	0.033	0.014	32	2.322	0.029	0.012
C_U/C_I	49	4.82	0.13	0.026	32	4.61	0.16	0.036
C_B/C_V	50	1.6872	0.0064	0.0038	33	1.6805	0.0061	0.0036
C_B/C_R	50	3.5206	0.029	0.0082	33	3.4573	0.030	0.0088
C_B/C_I	44	6.80	0.23	0.035	32	6.60	0.31	0.048
C_V/C_R	57	2.077	0.011	0.0051	40	2.049	0.012	0.0056
C_V/C_I	57	4.14	0.11	0.026	40	4.00	0.15	0.037
C_R/C_I	57	1.992	0.051	0.026	40	1.954	0.073	0.037

Notes. $C_{\rm band}$'s are in units of erg s^{-1} cm^{-3}. Distribution standard deviations (σ) can be obtained by multiplying standard errors of the mean (σ_m) by $\sqrt{N}$.
[a] Standard *uvby* magnitudes extracted from Hauck & Mermilliod (1998).
[b] Standard *UBV* magnitudes extracted from Mermilliod (1997).
[c] Standard Johnson *UBV RI* magnitudes extracted from Lanz (1986).

Table 2
$C_{\rm band}$'s and $C_{\rm band}$ Ratios for Individual Stars

Name	C_1	C_2	C_3	C_4	C_5	C_1/C_2	C_1/C_3	C_1/C_4	C_1/C_5	C_2/C_3	C_2/C_4	C_2/C_5	C_3/C_4	C_3/C_5	C_4/C_5
						uvby Bands									
HD 166	1.28823	0.90410	0.61248	0.38130	. . .	1.42487	2.10331	3.37850	. . .	1.47614	2.37108	. . .	1.60628	. . .	. . .
. . .															
HD 225261	1.03077	0.80285	0.57863	0.37351	. . .	1.28388	1.78140	2.75965	. . .	1.38751	2.14946	. . .	1.54915	. . .	. . .
						UBV Bands									
HD 166	0.46008	0.65767	0.37730	. . .	. . .	0.69956	1.21941	. . .	. . .	1.74311	. . .	. . .	. . .	. . .	. . .
. . .															
HD 224383	0.41801	0.60552	0.35786	. . .	. . .	0.69034	1.16810	. . .	. . .	1.69207	. . .	. . .	. . .	. . .	. . .
						UBV RI Bands									
HD 3651	0.42350	0.61044	0.35983	0.17395	0.08676	0.69376	1.17695	2.43460	4.88143	1.69648	3.50929	7.03620	2.06858	4.14754	2.00502
. . .															
HD 222368	0.42273	0.61846	0.36631	0.18023	0.08595	0.68352	1.15403	2.34553	4.91841	1.68837	3.43156	7.19573	2.03248	4.26195	2.09692

Note. Numeral subscripts refer to the bands applicable for each set. $C_{\rm band}$'s are in units of erg s^{-1} cm^{-3}.

(This table is available in its entirety in a machine-readable form in the online journal. A portion is shown here for guidance regarding its form and content.)
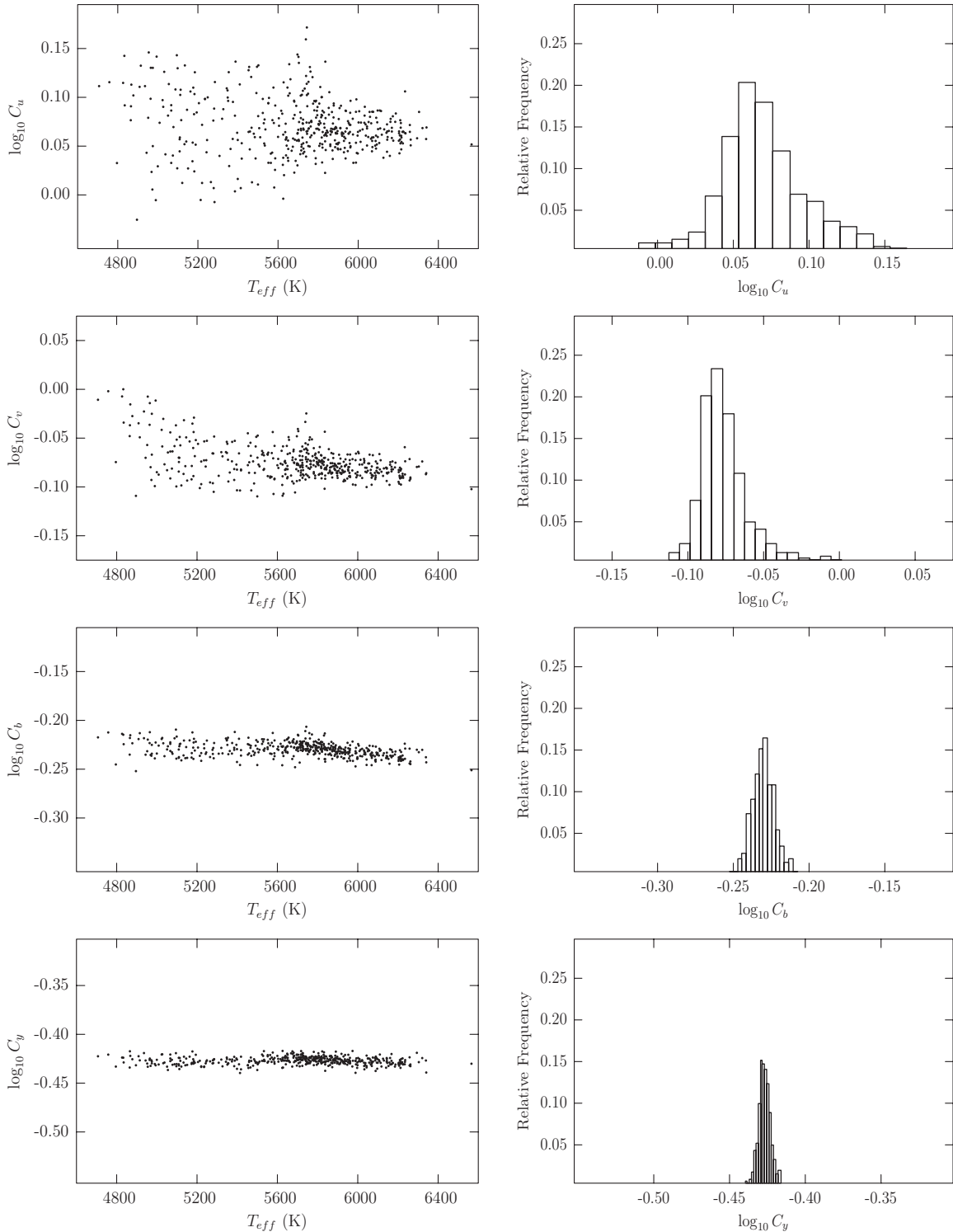
Figure 1. Strömgren u, v, b, y calibration constants vs. temperature (left) and histograms (right) for the 462 single stars of data set 1 in Table 1.

about $T = 5300$ K are systematically offset in Strömgren C_v and in Johnson C_U, C_R, and C_I. Of course, similar offsets appear in C_{band} ratios that contain those C_{band}'s. We do not know the specific reasons for these effects but they may be related to spectral features and blanketing. Shifts in the means due to this phenomenon are small, although perhaps not negligible.

Clues to the main error sources are in Figures 1–10, which show logarithmic C_{band}'s and C_{band} ratios versus temperature for hundreds of single stars (see Table 1), as computed from

Equations (1) and (2). The abscissa and ordinate scales have been chosen to facilitate inter-comparison of noise patterns, with the plots having identical temperature scales and all the logarithmic C_{band} and C_{band} ratio scales having the same spacings. A given percent noise corresponds to the same scatter-band width for all the plots as a consequence of the logarithmic scales with strictly fixed intervals. The noise is illustrated by many figures because visual comparison conveys a sense of accuracy and precision much more readily than reading
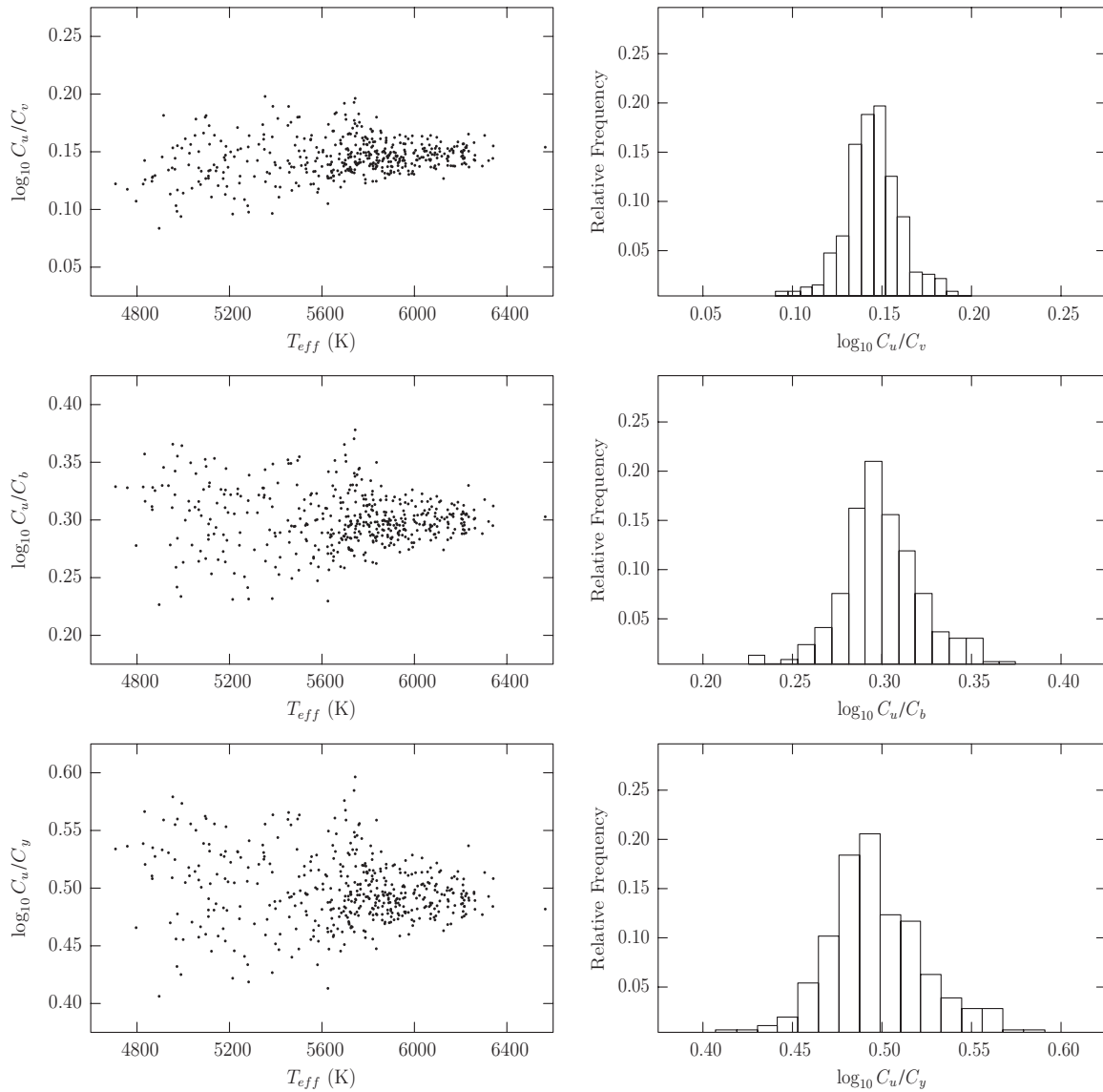
Figure 2. Calibration ratios C_u/C_v, C_u/C_b, and C_u/C_y vs. temperature (left) and histograms (right) for the 462 single stars of data set 1 in Table 1.

of tabulated numbers. One sees immediately that there are (currently unexplained) asymmetries in the histograms and dependences on temperature, while the Sun's locations show essential agreement (or in a few cases slight disagreement) with the single star results. It may seem unnecessary to include figures for C_{band} ratios that are not formally independent of other plotted ratios, such as C_v/C_b when there are figures for C_u/C_v and C_u/C_b. However, the extra figures are helpful in showing where random and systematic effects lie (are they mainly in C_u, C_b, or C_v?).

We find C_{band} ratios that differ from star to star, with strongly band-dependent standard deviations that range from about 2% in C_b/C_y to about 10% in C_u/C_y and C_U/C_V. Because C_{band} ratios are nearly independent of R and d, as shown by Equation (2), possible sources for most of the scatter in the ratios are the observed color indices and estimated temperatures, both of which produce larger scatter at shorter wavelengths.[9] In a simple numerical experiment, input temperatures were altered

by a few hundred Kelvins to see the relative changes in C_U and C_V, with resulting C_U changes being about 1.4 times larger than C_V changes, percent wise. Since (percent) C_U σ's are about 5 times larger than C_V σ's, any errors in estimated temperature cannot contribute more than a small part of the scatter in C_U. By process of elimination, the only noise source that can account for most of the scatter at the shorter wavelengths is photometry. Naturally, averages based on hundreds of stars will greatly reduce accidental error.[10]

As shown by Equation (1), derived calibrations are based on measured star magnitudes (m) that implicitly depend on true instrumental response functions and on theoretical fluxes (f) that depend on adopted response functions. The adopted functions are proxies for the realistically unknowable true functions that can differ significantly among data sets. Some published C_{band}'s differ from those of this paper mainly due to adopted response functions. For example, our several estimates of C_B in this and later sections cluster around 0.62 erg s^{-1} cm^{-3}, while Johnson (1965a) and Bessell (1979) give 0.69 and 0.66 erg s^{-1} cm^{-3},

---

[9] Earth atmosphere extinction (in optical bands) increases steeply toward shorter wavelengths and temperature affects stellar emission more strongly toward shorter wavelengths.

[10] Note that Equation (1) can usefully estimate R after an accurate C_{band}, temperature, and distance have been established.
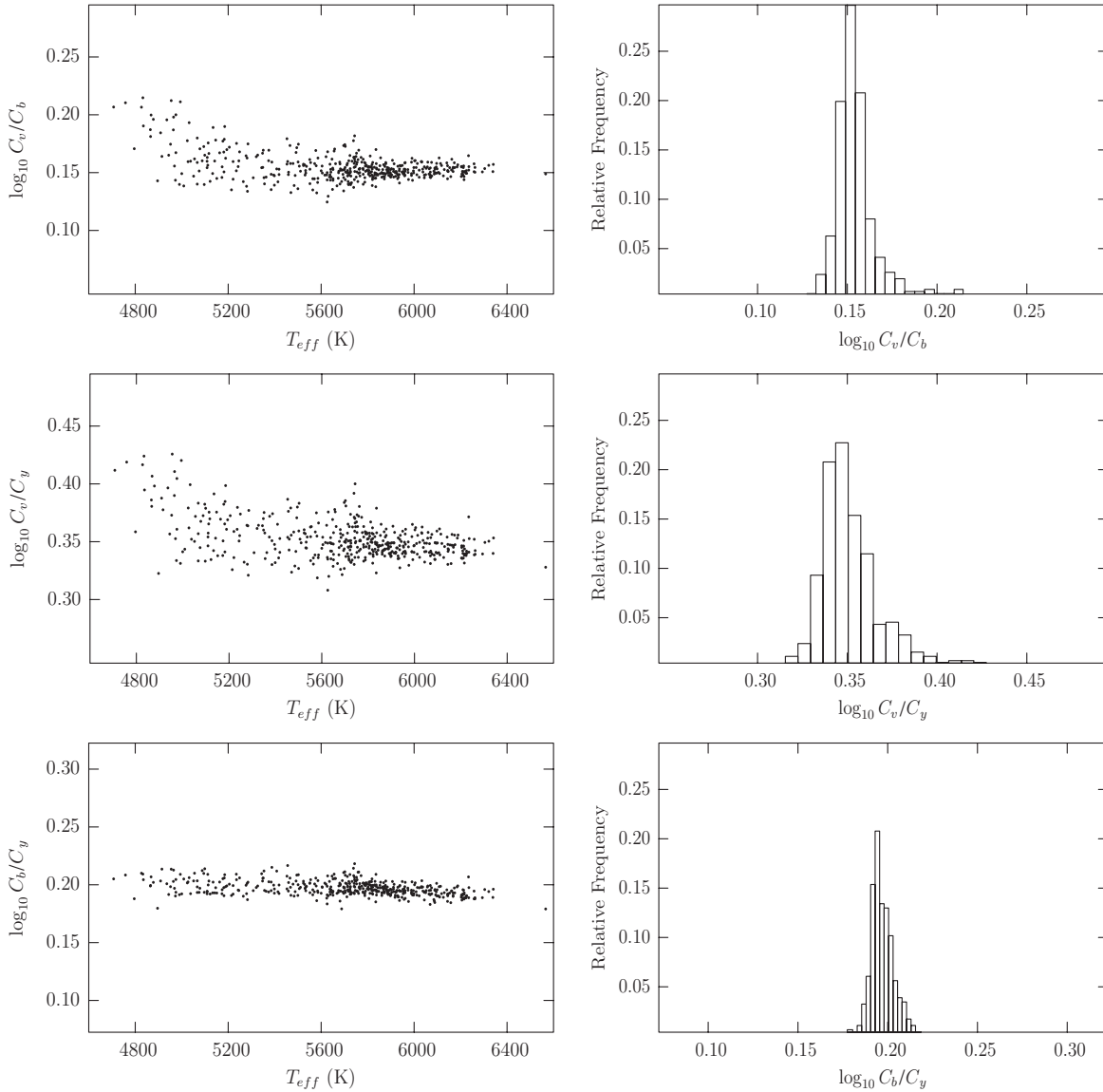
Figure 3. Calibration ratios C_v/C_b, C_v/C_y, and C_b/C_y vs. temperature (left) and histograms (right) for the 462 single stars of data set 1 in Table 1.

respectively, but the discrepancy is understandable in that our adopted B response (Ažusienis & Straižys 1969) is shifted noticeably with respect to theirs. One sees only small differences in mean estimated C_{band}'s where adopted response functions nearly agree. Accordingly, our C_{band}'s should be regarded as pertaining to the response functions adopted for the WD program (Ažusienis & Straižys 1969; Buser 1978; Crawford & Barnes 1970; Johnson 1965b; Bessell 1983).

2.3. The Sun and Interferometrically Observed Stars

In the case of negligible extinction, individual C_{band}'s could be measured accurately from standard magnitudes of a single star if R/d were somehow known with very small uncertainty, although the Sun may be the only star to meet that requirement. The main issue for the Sun is that its enormous brightness makes standard magnitudes difficult to measure. While recognizing that potential problem, we ran through the computation with input of solar *UBV RIK* apparent magnitudes from Cox (2004, p. 341) and output of the C_{band}'s and ratios in Table 3. The numbers for the Sun agree very closely with the single star averages of Table 1, although they are from completely

independent data. Table 3 has no σ's because we do not know the uncertainties of the solar magnitudes but, judging from the C_{band} agreements with the single star means, the Sun magnitudes in Cox (2004, p. 341) must be remarkably accurate.

The $(R/d)^2$ factor in Equation (1) suggests that interferometry may be useful for individual C_{band} measures by providing angular radii, although interferometry will not help for C_{band} ratios since R/d is absent from Equation (2). We examined the CADARS stellar interferometry catalog by Pasinetti Fracassini et al. (2001), looking for nearby stars with relatively good angular radii, standard magnitudes, and temperature estimates. We did not check the entire catalog of over 13,000 measures, but none of the nearby and clearly single stars such as Vega, Sirius A, τ Ceti, and ϵ Eridani that we checked gave C_B's or C_V's via Equation (1) in good agreement with values from other kinds of data. One would expect this result from scatter among individual interferometric R/d's that suggests 1σ uncertainties of order 5% in R/d (so 10% in $[R/d]^2$) in the better examples. However, prospects for interferometric C_{band} measurement, for example, by averaging results for many stars, should be examined more thoroughly.
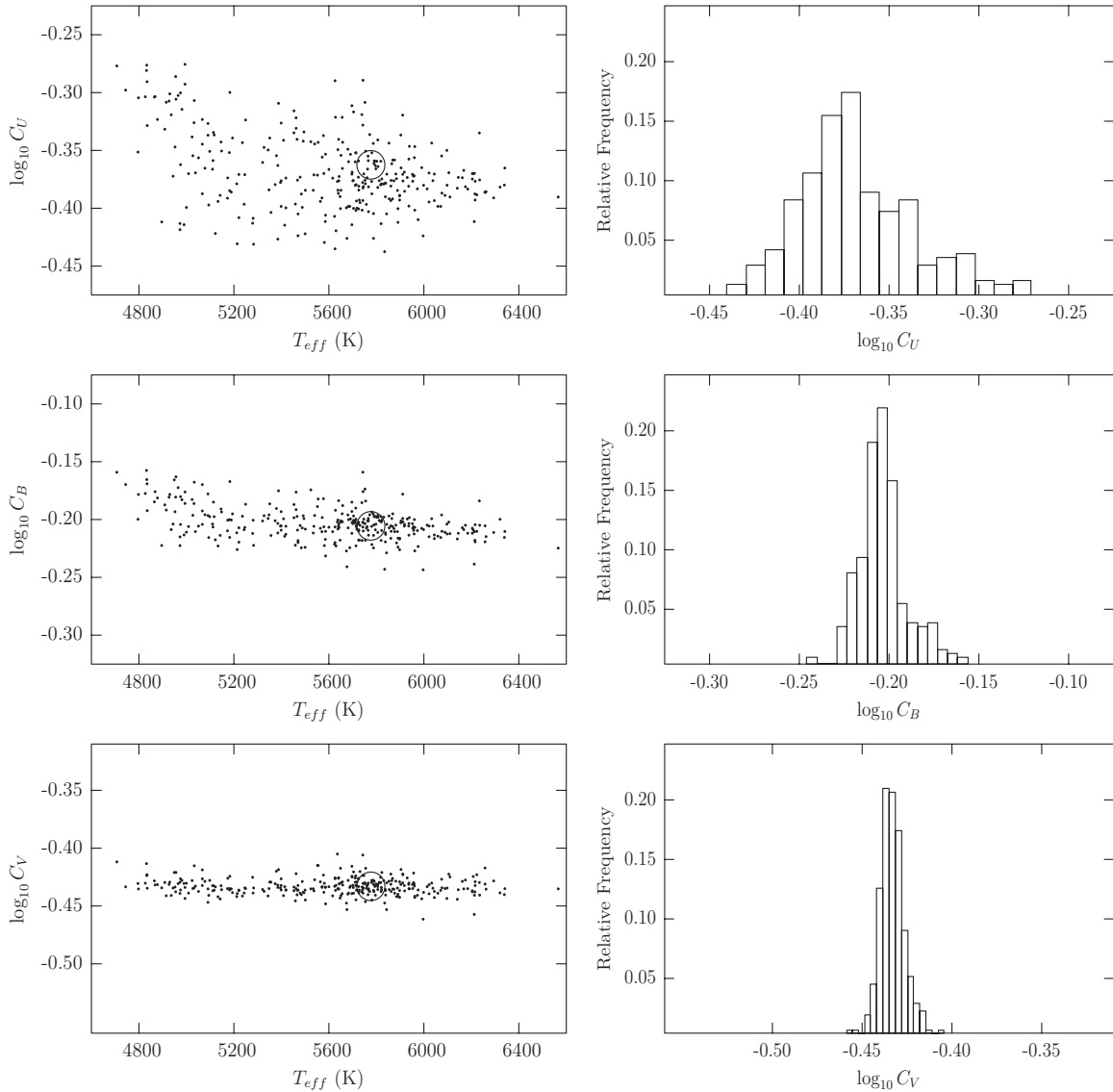
Figure 4. Johnson U, B, V calibration constants vs. temperature (left) and histograms (right) for the 310 single stars of data set 2 in Table 1. The Sun's position is shown by a circle.

2.4. Eclipsing Binaries versus Single Stars for Calibration Ratios

A single star with known or negligible interstellar extinction can offer physical and computational simplicity for C_{band} ratio estimation, only requiring a good color index in the relevant bands, approximately correct $\log g$, and approximately correct [M/H]. These are entered into a short program based on Equation (2) that directly calculates a C_{band} ratio without iteration. The advantage of single star targets is that C_{band} ratio results are independent of distance and not very sensitive to mass, radius, or composition. The down side is that each star must be effectively single, while it can be difficult to establish that no significantly luminous companion has affected the results (done here by requiring very small to nil RV variation). Similarly, an EB candidate ideally should lack a significantly luminous companion, although third light is an ordinary EB parameter that is routinely evaluated in light curve solutions. Also, companions to EBs can be detected by use of eclipses as timing ticks that quantify orbital motion about the barycenter, although that option is observationally intensive. Masses, radii,

and consequently also $\log g$'s are typically measured with good accuracy in EB solutions.

The most common reason for the shortfall of EB candidates, notwithstanding hundreds of nominal EBs in the solar neighborhood, is that the requisite observations have not been made. Also, many supposed EBs that have been reasonably well observed turn out to be ellipsoidal variables or have such shallow partial eclipses as not to be very useful for EB analysis. Many potentially good targets have good light curves but no RVs or RVs but no light curves, while others have good observations of both kinds but with RVs for only one component. Light curves of still others are not on standard photometric systems and not transformable to standard systems for one or more of several reasons. Although standard magnitudes of a comparison star are usually known and ostensibly standard filters may have been used, it may not be clear whether the differential light curves were properly transformed to standard systems. That problem may not be significant if the EB and its comparison star are nearly the same color and the EB's color is nearly constant, or if the instrumental and standard systems are very close to one another, but often the realistic situation cannot be ascertained
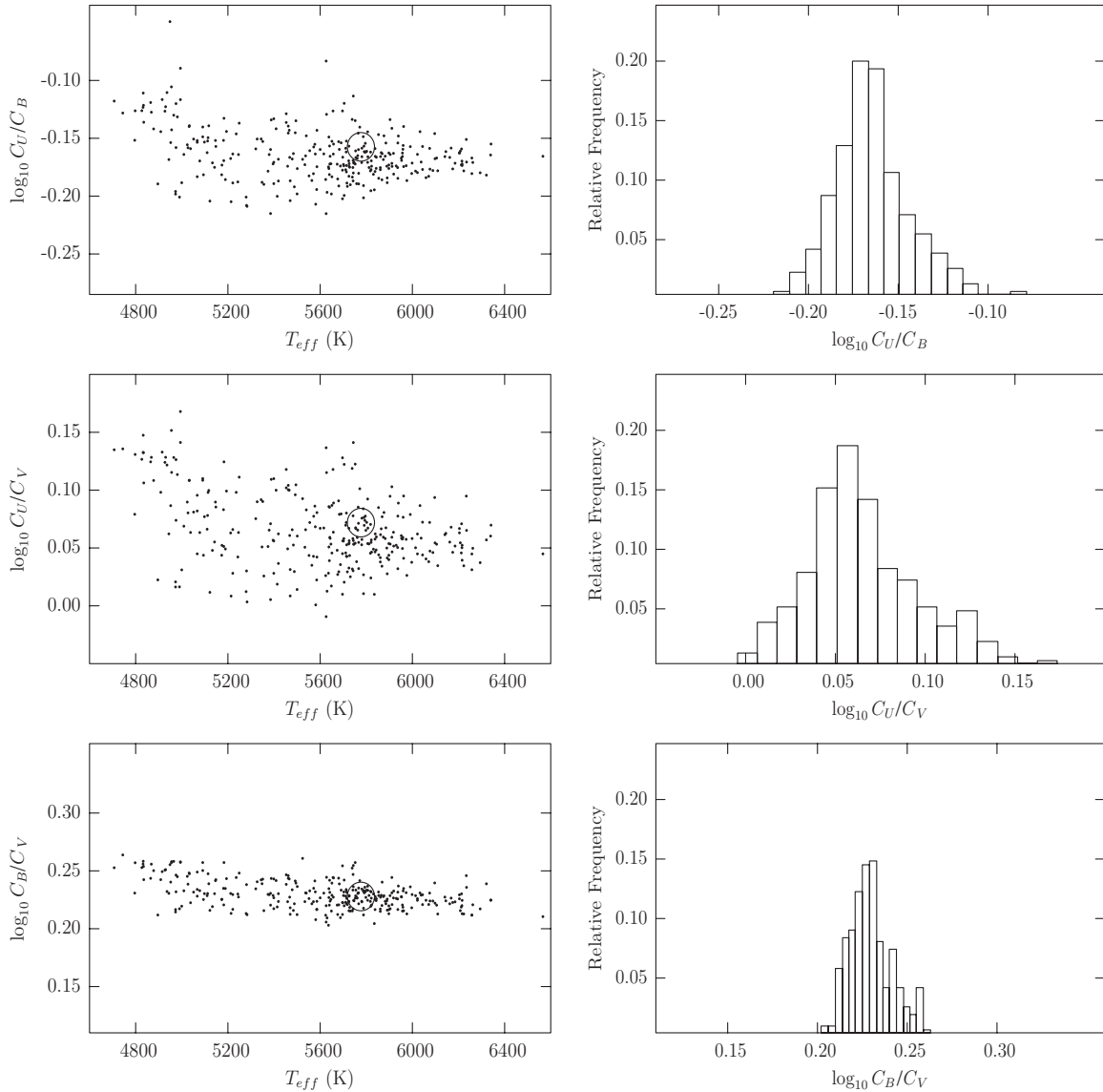
Figure 5. Calibration ratios C_U/C_B, C_U/C_V, and C_B/C_V vs. temperature (left) and histograms (right) for the 310 single stars of data set 2 in Table 1.

from an observational paper. Standardization uncertainties have little impact on traditional non-absolute EB solutions, but do impact absolute solutions, as they correspond to physical flux errors. The many light curves that are reported and perhaps shown graphically in papers, but not published in useful form, detract further from the candidate list. Finally, we avoided EBs with substantial third light. In our experience, third light of the order of a few percent of system light does not degrade essential results significantly, but amounts of the order of 20% or more may do so. On the positive side, comparison star standard magnitudes are now commonly available thanks to networks of standard stars, e.g., Landolt (1992, 2007, 2009).

3. EB DIFFERENTIAL CORRECTIONS SOLUTIONS FOR CALIBRATION CONSTANTS

3.1. The Problem in Overview

The Differential Corrections (DC) algorithm equates a set of residuals, $\Delta f = f_O - f_C$, for an observable quantity f (one residual for each observation), to a sum of what might be called *partial residuals* or perhaps *individual parameter residuals*. One presumes that the partial residuals would add to the overall residual in f if observational error were absent and the linear approximation were entirely adequate. Subscripts O and C, respectively, mean "observed" and "computed" (from a model). In this context, the linear approximation means that only the first derivative term in the Taylor series of corrections is applied for each parameter, so iteration is required. Accordingly, the equation of condition for a least-squares application to n parameters ($p_i, i = 1, \ldots, n$) can be written

$$\Delta f = \frac{\partial \Delta f}{\partial p_1} \delta p_1 + \frac{\partial \Delta f}{\partial p_2} \delta p_2 + \ldots + \frac{\partial \Delta f}{\partial p_n} \delta p_n, \qquad (3)$$

where the δp's are differences between momentarily adopted and least-squares p's. Often one sees the partial derivatives written in terms of only f_C rather than $f_O - f_C$ because the f_O's are constants in most applications (i.e., the observations are definite and not subject to variation, thus not contributing to the derivatives). However, the partial derivatives needed for C_{band} adjustment differ from the other DC partials in that they come from variation of f_O rather than f_C. Given that $f_O = 10^{-0.4 m} \times C_{\text{band}}$, with m being stellar magnitude, the
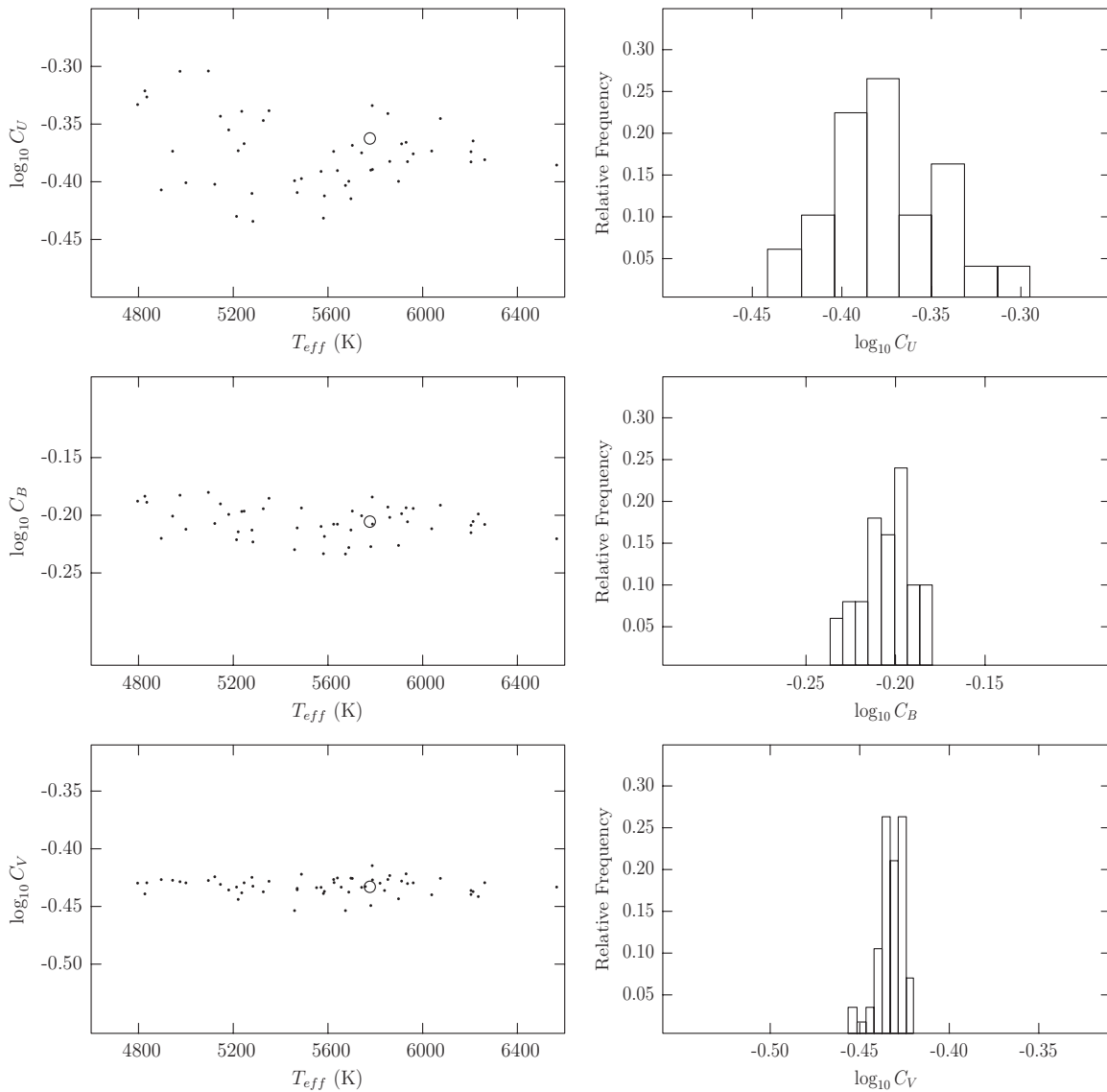
Figure 6. Johnson U, B, V calibration constants vs. temperature (left) and histograms (right) for the single stars of data set 3 in Table 1. The Sun's position is shown by a circle.

C_{band} derivative is just $\partial\Delta f/\partial C_{\mathrm{band}} = -10^{-0.4\,m}$ if expressed in magnitude or $\partial\Delta f/\partial C_{\mathrm{band}} = -f_O(m)/f_O$ ($m = 0$) if expressed in light (i.e., flux at Earth). Usually an implicit sign reversal is incorporated into the derivatives because one wants δp to represent a parameter correction rather than a parameter error. There is another reversal because of the minus sign attached to f_C, so the two sign reversals effectively leave a derivative's overall sign unchanged. For C_{band} derivatives, however, we differentiate f_O rather than f_C so there is only one sign reversal, thus reversing the overall sign of $\partial\Delta f/\partial C_{\mathrm{band}}$.

3.2. Input Temperature from Color Index

The EB-based calibrations of this paper are from least-squares solutions that require prior temperature estimates for one component and solve for the other temperature (and, of course, for C_{band}). In all cases, the prior-estimated temperature was that of star 1 (T_1) while the solution temperature was T_2. For binaries whose spectral-type information was not considered fully reliable, the prior T_1's were based on $B - V$ outside eclipse. A practical problem arises when a T_1 estimate is made from a

published color index that pertains to an entire EB—how are the components' flux contributions to be separated? The issue of which star is hotter will usually be clear from eclipse depths, but an intuitive guess of T_1 based on a T versus $B - V$ relation for single stars may be inaccurate. A partial accommodation adopted here is to tabulate EB solutions for several input T_1's so as to gauge how strongly the C_{band}'s and C_{band} ratios depend on T_1, but naturally one would like the middle of the T_1 range to be close to correct. Accordingly, prior T_1's were based on a consensus of published temperature calibrations, along with computational logic to account for the EBs being two-temperature sources. The relation between observable light (ℓ) and $B - V$ for a pair of simple spherical stars may be written as

$$\frac{(\ell_1 + \ell_2)_B}{(\ell_1 + \ell_2)_V} = 10^{0.4(K_{BV} - (B-V))}, \qquad (4)$$

where K_{BV} is the constant required by the condition that $B - V = 0$ for an average A0 V star, according to photometric convention. By numerical experiment with Kurucz (1993) atmosphere fluxes, we found that a K_{BV} of $+0.615$ approximately
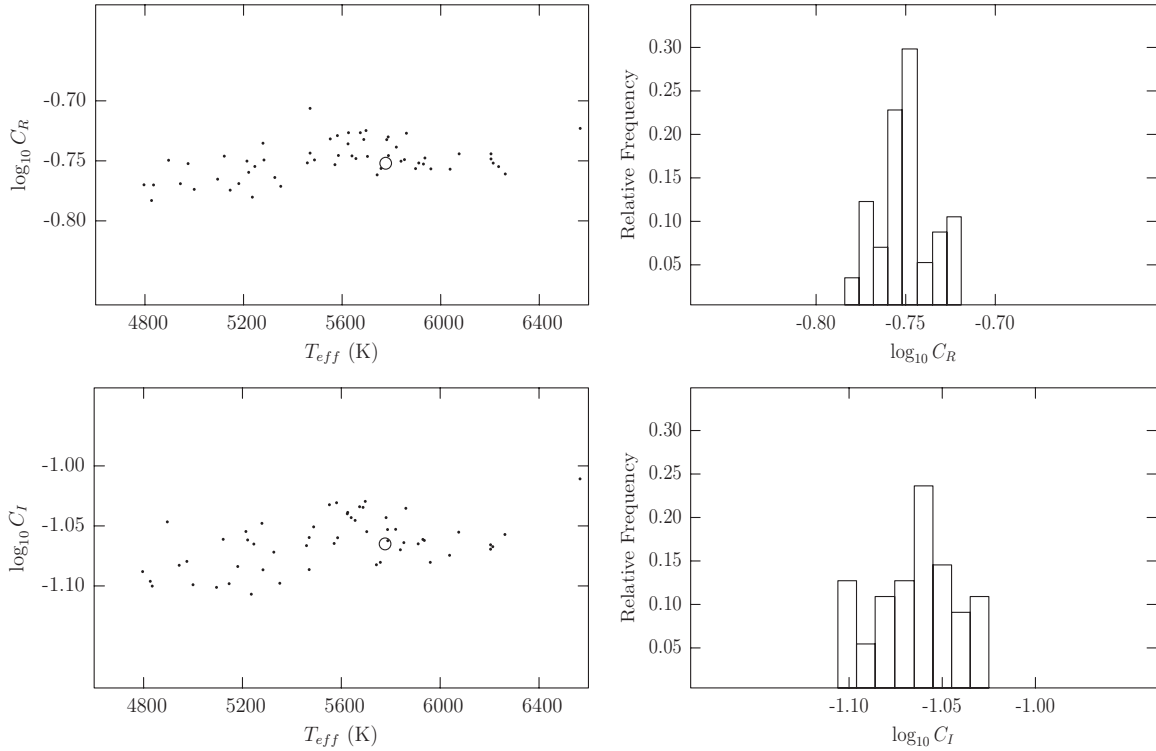
Figure 7. Johnson R, I calibration constants vs. temperature (left) and histograms (right) for the single stars of data set 3 in Table 1. The Sun's position is shown by a circle.

Table 3
C_{band}'s and C_{band} Ratios for Solar Data

Band or Band Ratio	Value
C_U (erg s^{-1} cm^{-3})	0.434
C_B (erg s^{-1} cm^{-3})	0.623
C_V (erg s^{-1} cm^{-3})	0.369
C_R (erg s^{-1} cm^{-3})	0.177
C_I (erg s^{-1} cm^{-3})	0.0861
C_K (erg s^{-1} cm^{-3})	0.00439
C_U/C_B	0.696
C_U/C_V	1.18
C_U/C_R	2.45
C_U/C_I	5.04
C_U/C_K	98.8
C_B/C_V	1.69
C_B/C_R	3.52
C_B/C_I	7.23
C_B/C_K	142
C_V/C_R	2.09
C_V/C_I	4.29
C_V/C_K	84.0
C_R/C_I	2.05
C_R/C_K	40.3
C_I/C_K	19.6

satisfies Equation (4) for main-sequence star data. The temperature data upon which K_{BV} is based are from Table 15.7 of Cox (2004, p. 341) and from approximation formulae by Casagrande et al. (2006, 2008, 2010). Once K_{BV} has been set to agree with those relations on average, Equation (4) can extend the relations' usefulness to stars outside the original temperature range. The left side of Equation (4) is designated S_{atm} and the right side S_{obs}, as they come, respectively, from stellar atmosphere output and observations. A preliminary non-absolute EB solution provides

star radii and a $T_2(T_1)$ relation that comes mainly from eclipse depths so as to allow iterative computation of the ℓ's and thus S_{atm} as the momentarily estimated T_1 varies. Since only a small range of T_1 is involved, the relation usually can be as simple as $T_2 = \text{constant} \times T_1$. We then seek an iterative solution for the implicit T_1 that leads to $S_{obs} - S_{atm} = \Delta S = 0$, where S_{obs} need be computed only once for each binary. The iterations begin from a preliminary T_1 for which ΔS and $\partial(\Delta S)/\partial T_1$ are computed via stellar atmosphere fluxes (see Van Hamme & Wilson 2003), and then T_1 is corrected by

$$\Delta T_1 = \frac{\Delta S}{\left(\frac{\partial(\Delta S)}{\partial T_1}\right)}. \qquad (5)$$

Typically, three to five iterations find a definite T_1 within a pre-set tolerance that can be very small.

3.3. Weighting in Simultaneous Solutions

Curve-dependent weighting can be important in simultaneous least-squares solutions of multiple curves. The DC program follows rules in Wilson (1979) that apply curve-dependent weights by input of an estimated standard deviation (σ) for each velocity and light curve. Of course only σ ratios matter, not the individual values. Our practice is to begin with initial estimates and refine the σ's as the iterations proceed, with one or two revisions usually adequate. Experience shows that modest disagreements between estimated and actual σ ratios, say by factors of two or so, do not much affect parameter results. However, σ ratios that are off by orders of magnitude can seriously degrade results and even cause some curves to be essentially ignored, so the σ's should be evaluated conscientiously.
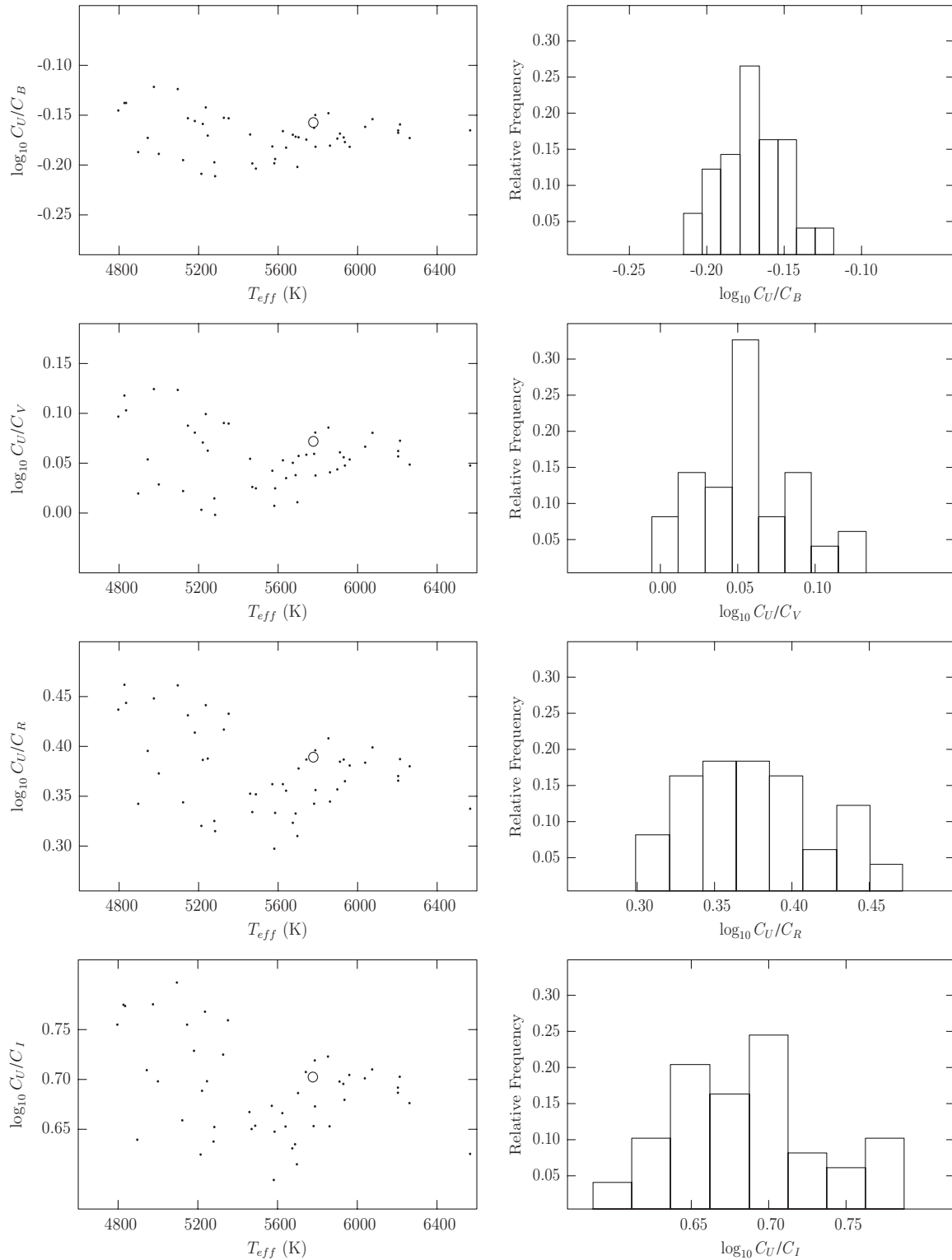
Figure 8. Calibration ratios C_U/C_B, C_U/C_V, C_U/C_R, and C_U/C_I vs. temperature (left) and histograms (right) for the single stars of data set 3 in Table 1. The Sun's position is shown by a circle.

4. CALIBRATION EB STRATEGIES, TARGETS, AND RESULTS

The EB protocol for C_{band} solutions was in two steps, with a non-absolute solution for most parameters followed by an absolute solution for only T_2, the calibrations, and third lights. It was the same for all binaries of this paper, except that most solutions did not need third light, and is justified as follows. To

begin, orbit size has no effect on theoretical light curve fluxes (ℓ) in non-absolute computations, as the intent is to represent arbitrarily scaled observations, so semimajor axis length (a) is purely an RV parameter in that case ($\partial\ell/\partial a = 0$). Accordingly, orbit size cannot be found from arbitrarily scaled light curves alone. However, the situation is entirely different for absolute light curve solutions. With other parameters fixed, including relative star sizes $r_{1,2} = R_{1,2}/a$, observable flux scales with
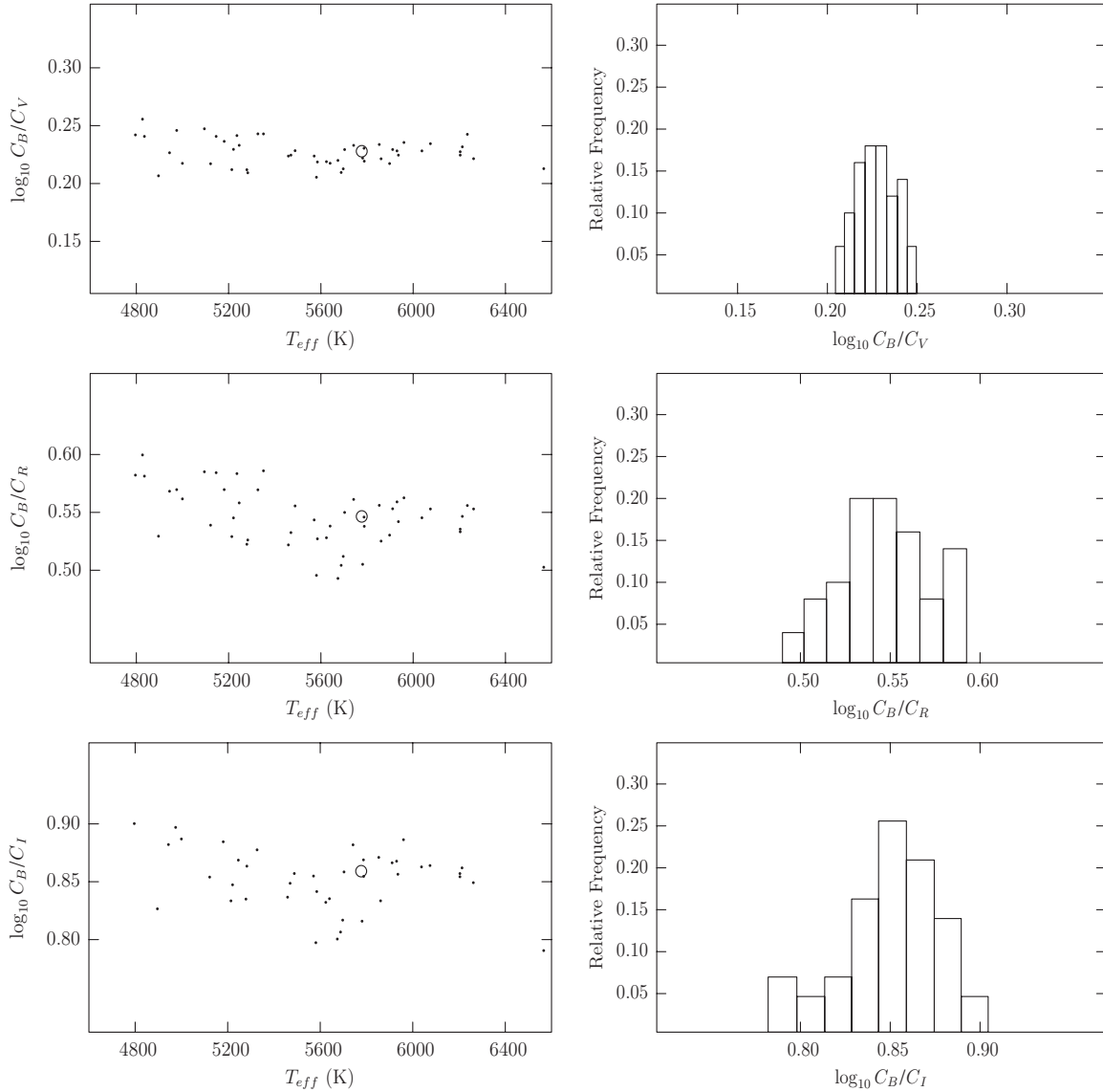
Figure 9. Calibration ratios C_B/C_V, C_B/C_R, and C_B/C_I vs. temperature (left) and histograms (right) for the single stars of data set 3 in Table 1. The Sun's position is shown by a circle.

a^2 since star size scales with a, so parameter a is derivable from one or more absolute light curves, given d. Note that the influence of d is not minor—with all else ideal, a 10% wrong distance will produce a 10% error in orbit size and $\approx 20\%$ C_{band} error. The point is that one should not try to find parameter a from an absolute light curve solution unless there is no other way or unless d is somehow known with unusually good (basically unprecedented) accuracy. Derived C_{band}'s depend strongly on a and d, so simultaneous (RV, absolute light) solutions will produce compromise calibrations based on both kinds of data, with wrong d leading to wrong a, which leads in turn to wrong calibrations. Realistic situations can be made worse by greatly unequal sizes and precisions of typical RV and light curve data sets, with light curves usually winning easily on both quantity and quality. Having 50 times as many light curve data points as RV points is not unusual. To deal with this circumstance, we begin by finding most parameters, including a, in a traditional (non-absolute) solution so as to ensure that "light curve a's" do not influence derived C_{band}'s. The idea is to evaluate most parameters from a non-absolute solution, leaving only T_2, C_{band}'s, and ℓ_3's for the absolute solution. Our experience is that T_2 changes only slightly between the non-absolute and absolute solutions. Parameter ℓ_3 is re-adjusted in the absolute solution because the flux unit differs between the non-absolute and absolute cases. Experiments show that the absolute light-RV solutions for fixed d produce very nearly the same C_{band}'s whether carried out simultaneously or in each band separately, so they were done simultaneously.

EBs chosen here for calibration analyses have good RV and light curve observations on standard photometric systems, circumstances well suited to strong solutions (mainly reasonably deep eclipses), and absence of strongly irregular behavior. The discussion of common shortcomings in Section 2.4 is in no way meant to imply lack of other good candidates, and interested persons can certainly add meaningfully to EB-based C_{band}'s. Although good traditional (i.e., non-absolute) solutions for all seven of this paper's "calibration" EBs are in the literature, our full parameter results are tabulated so as to place the derived calibrations in proper context. The numbers are in solution Tables 4–10 for TZ Men, V1130 Tau, TY Pyx, V505 Per, ε CrA, BG Ind, and WW Aur, respectively. The distances in all these tables are fixed input taken from the revised HIP catalog
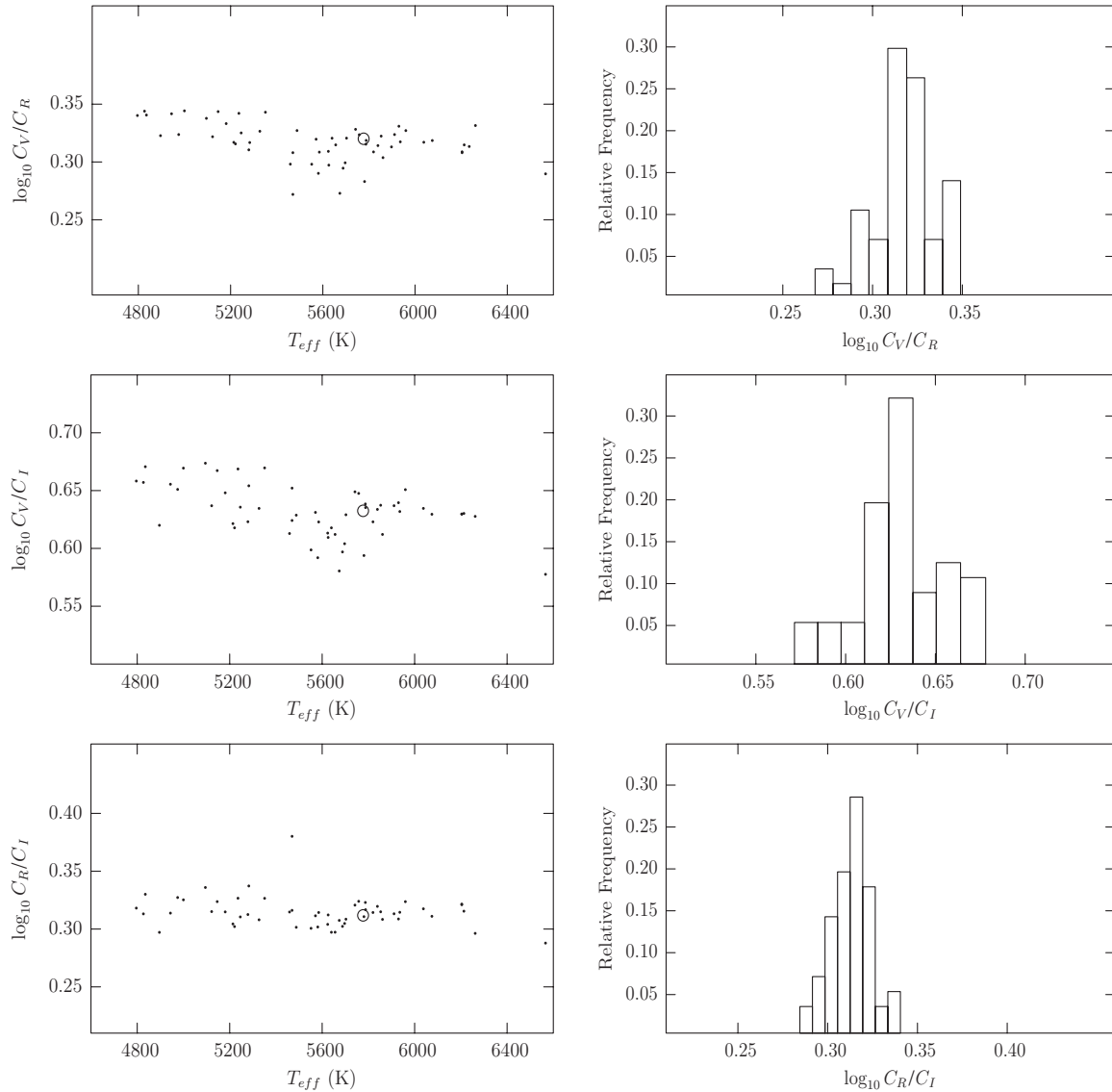
Figure 10. Calibration ratios C_V/C_R, C_V/C_I, and C_R/C_I vs. temperature (left) and histograms (right) for the single stars of data set 3 in Table 1. The Sun's position is shown by a circle.

(van Leeuwen 2007). Third light was negligible (below 1σ) or slightly negative and set to zero in final iterations, except for ϵ CrA and WW Aur. References for utilized RV and light curve data are in footnotes to the solution tables. The solutions were done in T_1 triplets for reasons given in Section 5. All of the RV observations are excellent, with tight fits, and good RV and light curve figures for these binaries are in the literature (follow the given references) so most of the RV's are not illustrated. The same is true for the light curves except for those of TY Pyx in Figure 11 and those of ϵ CrA in Figures 12–14 that illustrate fitting issues discussed in Sections 4.3 and 4.5. RV's for ϵ CrA are shown in Figure 14 because of scatter in the velocities of star 2.

4.1. TZ Mensae

TZ Mensae is a well-detached B9 IV-V EB with $V \approx 6.2$ mag, $d \approx 110$ pc, and a slightly eccentric, nearly edge-on orbit of period 8.57 days. A fixed input temperature of $T_1 = 10,437$ K was estimated for our calibration solutions via the scheme of Section 3.2, based on Equations (4) and (5). Metallicity, [M/H], was assumed to be zero. Although there is no evidence for

measurable period variation or apsidal motion, it was necessary to include the period and reference epoch in the solution rather than adopt one from the literature because published TZ Men ephemerides are specifically for the primary or secondary eclipse. All versions of the WD program, including DDE, work with ephemerides that are not specifically related to eclipses or to actual conjunctions but to conjunctions that occur when the orbital major axes are most nearly along the line of sight, with star 1 away from the observer (i.e., for argument of periastron $\omega_1 = \pi/2$ rad). The reason is to have computed eclipses make phase excursions due to apsidal motion in the same way as real eclipses (one goes left while the other goes right, and then they reverse motions), rather than have one eclipse at fixed phase while the other moves. A consequence for TZ Men of these contrasting concepts is that our reference time, T_0, differs by more than an hour from the one by Andersen et al. (1987), although our derived period is the same as theirs within stated uncertainties.

The Grønbech et al. (1987) light curves were made with the Danish 50 cm telescope at Cerro Tololo. The transformations by Grønbech et al. (1976) were applied to the differential

Table 4
TZ Men Parameters, C_{band}'s, C_{band} Ratios, and T_1 Dependence

p	T_1 (Low)	T_1 (Adopted)	T_1 (High)	$\partial p/\partial T_1$
d_{HIP} (pc)	...	112.2 ($\pm$3.1)	...	...
a ($R_\odot$)	...	27.771 $\pm$ 0.075	...	...
e	...	0.0364 $\pm$ 0.0009	...	...
ω (rad)	...	5.133 $\pm$ 0.011	...	...
V_γ (km s^{-1})	...	-0.27 ± 0.12	...	...
i (deg)	...	88.718 $\pm$ 0.032	...	...
Ω_1	...	14.464 $\pm$ 0.024	...	...
Ω_2	...	13.078 $\pm$ 0.033	...	...
M_2/M_1	...	0.6094 $\pm$ 0.0025	...	...
T_0 (HJD)	...	2442403.75028 $\pm$ 0.00015	...	...
P (days)	...	8.5689906 $\pm$ 0.0000015	...	...
dP/dt	...	$+6.8 \pm 1.4 \times 10^{-9}$	...	...
T_1 (K)	10407.0	10437.0	10467.0	...
T_2 (K)	7169 $\pm$ 6	7183 $\pm$ 6	7196 $\pm$ 6	...
C_u (erg s^{-1} cm^{-3})	1.2748 $\pm$ 0.0079	1.2897 $\pm$ 0.0080	1.3047 $\pm$ 0.0081	0.00050
C_v (erg s^{-1} cm^{-3})	0.9177 $\pm$ 0.0059	0.9249 $\pm$ 0.0060	0.9320 $\pm$ 0.0060	0.00024
C_b (erg s^{-1} cm^{-3})	0.6329 $\pm$ 0.0041	0.6371 $\pm$ 0.0041	0.6413 $\pm$ 0.0041	0.00014
C_y (erg s^{-1} cm^{-3})	0.4038 $\pm$ 0.0027	0.4063 $\pm$ 0.0027	0.4088 $\pm$ 0.0027	0.00008
C_u/C_v	1.389 $\pm$ 0.012	1.394 $\pm$ 0.013	1.400 $\pm$ 0.013	0.00018
C_u/C_b	2.014 $\pm$ 0.018	2.024 $\pm$ 0.018	2.035 $\pm$ 0.018	0.00034
C_u/C_y	3.157 $\pm$ 0.029	3.174 $\pm$ 0.029	3.192 $\pm$ 0.029	0.00058
C_v/C_b	1.450 $\pm$ 0.013	1.452 $\pm$ 0.013	1.453 $\pm$ 0.013	0.00006
C_v/C_y	2.273 $\pm$ 0.021	2.276 $\pm$ 0.021	2.280 $\pm$ 0.021	0.00012
C_b/C_y	1.567 $\pm$ 0.015	1.568 $\pm$ 0.015	1.569 $\pm$ 0.014	0.00002

Notes. Double-lined RVs are from Andersen et al. (1987), and *uvby* light curves are from Grønbech et al. (1987). The error in d is from van Leeuwen (2007), and not a solution error since d is a fixed parameter in this solution.

Table 5
V1130 Tau Parameters, C_{band}'s, C_{band} Ratios, and T_1 Dependence

p	T_1 (Low)	T_1 (Adopted)	T_1 (High)	$\partial p/\partial T_1$
d_{HIP} (pc)	...	68.7 ($\pm$2.3)	...	...
a ($R_\odot$)	...	5.0466 $\pm$ 0.0098	...	...
V_γ (km s^{-1})	...	-11.14 ± 0.25	...	...
i (deg)	...	73.629 $\pm$ 0.035	...	...
Ω_1	...	4.513 $\pm$ 0.011	...	...
Ω_2	...	4.0468 $\pm$ 0.0079	...	...
M_2/M_1	...	1.0651 $\pm$ 0.0037	...	...
T_0 (HJD)	...	2450770.696088 $\pm$ 0.000036	...	...
P (days)	...	0.79886815 $\pm$ 0.00000030	...	...
T_1 (K)	6786	6806	6826	...
T_2 (K)	6780 $\pm$ 2	6800 $\pm$ 2	6819 $\pm$ 2	...
C_u (erg s^{-1} cm^{-3})	1.4373 $\pm$ 0.0061	1.4592 $\pm$ 0.0063	1.4810 $\pm$ 0.0064	0.00109
C_v (erg s^{-1} cm^{-3})	1.0423 $\pm$ 0.0045	1.0610 $\pm$ 0.0046	1.0781 $\pm$ 0.0047	0.00090
C_b (erg s^{-1} cm^{-3})	0.7089 $\pm$ 0.0030	0.7192 $\pm$ 0.0031	0.7297 $\pm$ 0.0032	0.00052
C_y (erg s^{-1} cm^{-3})	0.4472 $\pm$ 0.0019	0.4527 $\pm$ 0.0020	0.4582 $\pm$ 0.0020	0.00028
C_u/C_v	1.3790 $\pm$ 0.0083	1.3753 $\pm$ 0.0084	1.3737 $\pm$ 0.0084	-0.00013
C_u/C_b	2.028 $\pm$ 0.012	2.029 $\pm$ 0.012	2.030 $\pm$ 0.013	0.00005
C_u/C_y	3.214 $\pm$ 0.019	3.223 $\pm$ 0.020	3.232 $\pm$ 0.020	0.00046
C_v/C_b	1.4703 $\pm$ 0.0089	1.4753 $\pm$ 0.0090	1.4775 $\pm$ 0.0091	0.00018
C_v/C_y	2.331 $\pm$ 0.014	2.344 $\pm$ 0.015	2.348 $\pm$ 0.015	0.00043
C_b/C_y	1.5852 $\pm$ 0.0095	1.5887 $\pm$ 0.0098	1.5891 $\pm$ 0.0098	0.00010

Notes. RVs and *uvby* light curves are from Clausen et al. (2010). The error in d is from van Leeuwen (2007), and not a solution error since d is a fixed parameter in this solution.

instrumental light curves, following advice from J. V. Clausen, although the transformations made only small changes in the final standardized light curves. Standard magnitudes for the comparison star, HD 40953 = κ Men, are from Table 1 of Andersen et al. (1987). Solution difficulties related to the eccentric orbit and narrow eclipses were confined to the early stages. Refinements and minor experiments went well after rough agreement was reached.

4.2. V1130 Tauri

A traditional analysis of V1130 Tauri, an EB with $V = 6.6$ mag and orbit period 0.80 days, has just appeared (Clausen et al. 2010), based on excellent newly published RV curves and *uvby* light curves. Our absolute solution for calibrations utilized the same data. The HIP distance is 70 pc, with a 3% standard error. Clausen et al. (2010) discussed the system's

Table 6
TY Pyx Parameters, C_{band}'s, C_{band} Ratios, and T_1 Dependence

p	T_1 (Low)	T_1 (Adopted)	T_1 (High)	$\partial p/\partial T_1$
Spot co-latitude (rad)	...	1.484	...	...
Spot longitude (rad)	...	4.000 ± 0.023	...	...
Spot angular radius (rad)	...	0.3491	...	...
Spot T-factor	...	0.9644 ± 0.0018	...	...
d_{HIP} (pc)	...	56.4 (±1.7)	...	...
a ($R_\odot$)	...	12.241 ± 0.047	...	...
V_γ (km s^{-1})	...	$+63.37 \pm 0.37$	...	...
i (deg)	...	87.773 ± 0.036	...	...
Ω_1	...	8.457 ± 0.018	...	...
Ω_2	...	8.434 ± 0.0032	...	...
M_2/M_1	...	0.9856 ± 0.0051	...	...
T_0 (HJD)	...	$2443187.23007 \pm 0.00049$	...	...
P (days)	...	3.1985799 ± 0.0000041	...	...
T_1 (K)	5647	5667	5687	...
T_2 (K)	5617 ± 1	5636 ± 1	5656 ± 1	...
C_u (erg s^{-1} cm^{-3})	1.1432 ± 0.0061	1.1801 ± 0.0096	1.2178 ± 0.0100	0.00187
C_v (erg s^{-1} cm^{-3})	0.8094 ± 0.0046	0.8310 ± 0.0067	0.8530 ± 0.0070	0.00109
C_b (erg s^{-1} cm^{-3})	0.5717 ± 0.0035	0.5833 ± 0.0047	0.5950 ± 0.0049	0.00058
C_y (erg s^{-1} cm^{-3})	0.3620 ± 0.0023	0.3683 ± 0.0031	0.3746 ± 0.0031	0.00032
C_u/C_v	1.412 ± 0.011	1.420 ± 0.016	1.428 ± 0.017	0.00038
C_u/C_b	2.000 ± 0.016	2.023 ± 0.023	2.047 ± 0.024	0.00118
C_u/C_y	3.158 ± 0.026	3.204 ± 0.038	3.251 ± 0.038	0.00233
C_v/C_b	1.416 ± 0.012	1.425 ± 0.016	1.434 ± 0.017	0.00045
C_v/C_y	2.236 ± 0.019	2.257 ± 0.026	2.277 ± 0.027	0.00104
C_b/C_y	1.579 ± 0.014	1.584 ± 0.019	1.588 ± 0.019	0.00023

Notes. Double-lined RVs are from Andersen & Popper (1975), and *uvby* light curves are from Andersen et al. (1981b). Spot co-latitude runs from 0 at the $+z$ pole to π radians at the $-z$ pole. Spot T-factor is the ratio of local in-spot T to no-spot T. Parameters with standard errors were adjusted. The error in d is from van Leeuwen (2007), and not a solution error since d is a fixed parameter in this solution.

Table 7
V505 Per Parameters, C_{band}'s, C_{band} Ratios, and T_1 Dependence

p	T_1 (Low)	T_1 (Adopted)	T_1 (High)	$\partial p/\partial T_1$
d (pc)	...	61.6 (±1.9)	...	...
a ($R_\odot$)	...	15.030 ± 0.021	...	...
V_γ (km s^{-1})	...	0.21 ± 0.09	...	...
i (deg)	...	87.897 ± 0.039	...	...
Ω_1	...	12.120 ± 0.093	...	...
Ω_2	...	12.88 ± 0.15	...	...
M_2/M_1	...	0.9874 ± 0.0025	...	...
T_0 (HJD)	...	$2451587.30590 \pm 0.00015$	...	...
P (days)	...	4.2220204 ± 0.0000024	...	...
T_1	6492	6512	6532	...
T_2 (K)	6443 ± 4	6463 ± 4	6483 ± 4	...
C_B (erg s^{-1} cm^{-3})	0.5806 ± 0.0042	0.5908 ± 0.0042	0.6012 ± 0.0043	0.00051
C_V (erg s^{-1} cm^{-3})	0.3594 ± 0.0026	0.3642 ± 0.0026	0.3690 ± 0.0026	0.00024
C_B/C_V	1.615 ± 0.017	1.622 ± 0.016	1.629 ± 0.016	0.00034

Notes. RV data and B, V light curves from Tomasella et al. (2008). The error in d is from van Leeuwen (2007), and not a solution error since d is a fixed parameter in this solution.

spectral type (early F), metallicity (for which we adopt [M/H] = -0.20), and particularly its somewhat evolved condition. The instrumental differential magnitudes are reportedly very close to the standard *uvby* systems, so the only requirement to form standard V1130 Tau magnitudes was to add in comparison star (HD 23503) magnitudes from Clausen et al. (2010).

Clausen et al. (2010) estimated a reference epoch and period from about 17 years of eclipse timings, finding no evidence for period change. Nearly the same ephemeris (see Table 5) came from our calibration solution with a time base of about

3.5 years (i.e., from entire RV and light curves rather than eclipse timings—see Wilson (2005) and Van Hamme & Wilson (2007) for specifics). Fixed input temperature T_1 was estimated via the scheme of Section 3.2. No significant solution difficulties were encountered. The C_{band}'s look high by an amount that corresponds to the (fixed input) HIP distance being low by about 11%. That would be a 3.4σ error, which is unlikely although not out of the question. However, the C_{band} ratios agree reasonably well with our single star means and solar values, as one would expect from the discussion of Equations (1) and (2) in Section 2.2.

Table 8
ϵ CrA Parameters, $C_{\rm band}$'s, $C_{\rm band}$ Ratios, and T_1 Dependence

p	T_1 (Low)	T_1 (Adopted)	T_1 (High)	$\partial p/\partial T_1$
d (pc)	$\ldots$	$30.18\ (\pm 0.30)$	$\ldots$	$\ldots$
$a\ (R_\odot)$	$\ldots$	3.721 ± 0.021	$\ldots$	$\ldots$
V_γ (km s^{-1})	$\ldots$	54.84 ± 0.52	$\ldots$	$\ldots$
i (deg)	$\ldots$	73.42 ± 0.12	$\ldots$	$\ldots$
Ω_1	$\ldots$	2.01171 ± 0.00084	$\ldots$	$\ldots$
Ω_2	$\ldots$	2.01171	$\ldots$	$\ldots$
M_2/M_1	$\ldots$	0.12260 ± 0.00016	$\ldots$	$\ldots$
T_0 (HJD)	$\ldots$	$2439707.663311 \pm 0.000059$	$\ldots$	$\ldots$
P (days)	$\ldots$	$0.59143373 \pm 0.00000020$	$\ldots$	$\ldots$
T_1 (K)	6500	6700	7000	$\ldots$
T_2 (K)	6124 ± 5	6305 ± 5	6576 ± 5	$\ldots$
ℓ_{3U} (10^{-4} erg s^{-1} cm^{-3})	4.05 ± 0.17	4.52 ± 0.19	5.25 ± 0.22	$\ldots$
ℓ_{3B} (10^{-4} erg s^{-1} cm^{-3})	5.20 ± 0.22	5.85 ± 0.23	6.91 ± 0.27	$\ldots$
ℓ_{3V} (10^{-4} erg s^{-1} cm^{-3})	3.36 ± 0.15	3.65 ± 0.16	4.12 ± 0.18	$\ldots$
ℓ_{3R} (10^{-4} erg s^{-1} cm^{-3})	1.13 ± 0.13	1.14 ± 0.14	1.17 ± 0.15	$\ldots$
ℓ_{3I} (10^{-4} erg s^{-1} cm^{-3})	0.492 ± 0.080	0.475 ± 0.085	0.447 ± 0.095	$\ldots$
C_U (erg s^{-1} cm^{-3})	0.4135 ± 0.0051	0.4950 ± 0.0059	0.6290 ± 0.0074	0.00043
C_B (erg s^{-1} cm^{-3})	0.5942 ± 0.0071	0.7032 ± 0.0083	0.889 ± 0.010	0.00059
C_V (erg s^{-1} cm^{-3})	0.3549 ± 0.0041	0.4032 ± 0.0046	0.4827 ± 0.0055	0.00026
C_R (erg s^{-1} cm^{-3})	0.1818 ± 0.0022	0.2011 ± 0.0024	0.2317 ± 0.0027	0.00010
C_I (erg s^{-1} cm^{-3})	0.0929 ± 0.0011	0.1007 ± 0.0012	0.1128 ± 0.0013	0.00004
C_U/C_B	0.695 ± 0.012	0.704 ± 0.012	0.707 ± 0.012	0.00002
C_U/C_V	1.165 ± 0.020	1.228 ± 0.020	1.303 ± 0.021	0.00028
C_U/C_R	2.274 ± 0.039	2.462 ± 0.042	2.715 ± 0.045	0.00088
C_U/C_I	4.451 ± 0.076	4.914 ± 0.083	5.577 ± 0.092	0.00225
C_B/C_V	1.674 ± 0.028	1.744 ± 0.029	1.843 ± 0.030	0.00034
C_B/C_R	3.268 ± 0.056	3.497 ± 0.059	3.839 ± 0.063	0.00114
C_B/C_I	6.40 ± 0.11	6.98 ± 0.12	7.89 ± 0.13	0.00298
C_V/C_R	1.952 ± 0.033	2.005 ± 0.033	2.084 ± 0.034	0.00026
C_V/C_I	3.820 ± 0.063	4.003 ± 0.066	4.280 ± 0.069	0.00092
C_R/C_I	1.957 ± 0.033	1.996 ± 0.034	2.054 ± 0.034	0.00019

Notes. RVs are by Goecking & Duerbeck (1993), *UBV* photometric data by Tapia (1969), and *RI* light curves by Hernández (1972). The error in d is from van Leeuwen (2007), and not a solution error since d is a fixed parameter in this solution.

Table 9
BG Ind Parameters, $C_{\rm band}$'s, $C_{\rm band}$ Ratios, and T_1 Dependence

p	T_1 (Low)	T_1 (Adopted)	T_1 (High)	$\partial p/\partial T_1$
d (pc)	$\ldots$	$67.1\ (\pm 2.7)$	$\ldots$	$\ldots$
$a\ (R_\odot)$	$\ldots$	7.715 ± 0.042	$\ldots$	$\ldots$
V_γ (km s^{-1})	$\ldots$	59.63 ± 0.56	$\ldots$	$\ldots$
i (deg)	$\ldots$	72.687 ± 0.095	$\ldots$	$\ldots$
Ω_1	$\ldots$	5.297 ± 0.041	$\ldots$	$\ldots$
Ω_2	$\ldots$	4.860 ± 0.024	$\ldots$	$\ldots$
M_2/M_1	$\ldots$	1.1298 ± 0.0051	$\ldots$	$\ldots$
T_0 (HJD)	$\ldots$	$2445907.94311 \pm 0.00023$	$\ldots$	$\ldots$
P (days)	$\ldots$	$1.46405868 \pm 0.00000039$	$\ldots$	$\ldots$
T_1 (K)	6430	6450	6470	$\ldots$
T_2 (K)	6059 ± 11	6077 ± 11	6094 ± 11	$\ldots$
C_u (erg s^{-1} cm^{-3})	1.020 ± 0.013	1.039 ± 0.013	1.059 ± 0.014	0.00098 ± 0.00047
C_v (erg s^{-1} cm^{-3})	0.7217 ± 0.0094	0.7355 ± 0.0096	0.7495 ± 0.0098	0.00069
C_b (erg s^{-1} cm^{-3})	0.5043 ± 0.0065	0.5121 ± 0.0066	0.5201 ± 0.0067	0.00040
C_y (erg s^{-1} cm^{-3})	0.3272 ± 0.0042	0.3315 ± 0.0043	0.3359 ± 0.0043	0.00022
C_u/C_v	1.413 ± 0.026	1.413 ± 0.026	1.413 ± 0.026	-0.00001
C_u/C_b	2.022 ± 0.037	2.029 ± 0.037	2.036 ± 0.037	0.00035
C_u/C_y	3.117 ± 0.057	3.135 ± 0.057	3.152 ± 0.057	0.00089
C_v/C_b	1.431 ± 0.026	1.436 ± 0.026	1.441 ± 0.026	0.00025
C_v/C_y	2.206 ± 0.040	2.219 ± 0.041	2.231 ± 0.041	0.00063
C_b/C_y	1.541 ± 0.028	1.545 ± 0.028	1.548 ± 0.028	0.00018

Notes. RVs from Bakiş et al. (2010) and *uvby* light curves from Mathys et al. (1986). The error in d is from van Leeuwen (2007), and not a solution error since d is a fixed parameter in this solution.
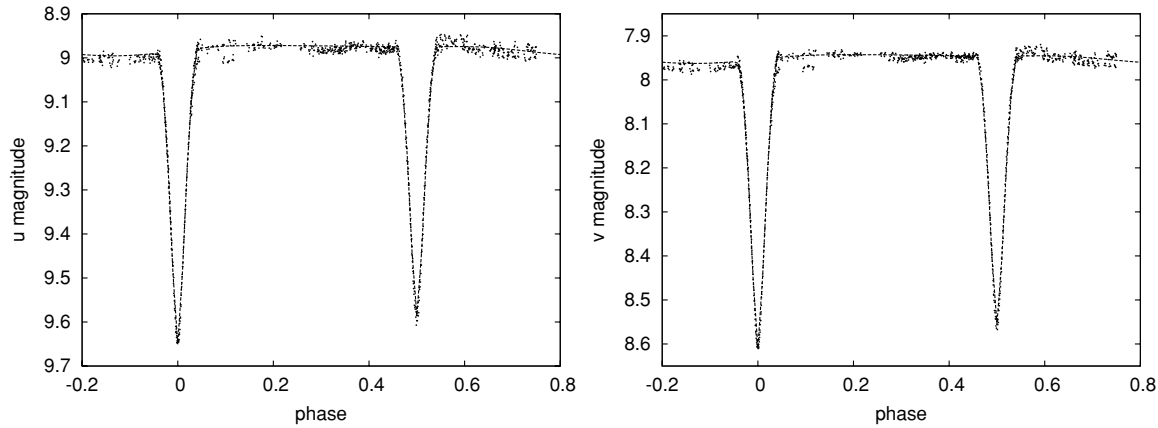
Figure 11. TY Pyx u (left) and v (right) curves for the $1T-C_{band}$ solutions of Section 4.3. Although spot modeling only partly succeeds in matching the observations, derived calibrations and calibration ratios are close to the single star means.

Table 10
WW Aur Parameters, C_{band}'s, C_{band} Ratios, and T_1 Dependence

p	T_1 (Low)	T_1 (Adopted)	T_1 (High)	$\partial p/\partial T_1$
d (pc)	...	80.6 ($\pm$2.3)	...	...
a ($R_\odot$)	...	12.204 $\pm$ 0.015	...	...
V_γ (km s^{-1})	...	-8.85 ± 0.13	...	...
i (deg)	...	87.670 $\pm$ 0.058	...	...
Ω_1	...	7.267 $\pm$ 0.020	...	...
Ω_2	...	6.931 $\pm$ 0.020	...	...
M_2/M_1	...	0.9202 $\pm$ 0.0018	...	...
T_0 (HJD)	...	2447259.87365 $\pm$ 0.00067	...	...
P (days)	...	2.52501902 $\pm$ 0.00000033	...	...
T_1	7980	8000	8020	...
T_2 (K)	7693 $\pm$ 2	7710 $\pm$ 2	7728 $\pm$ 2	...
ℓ_{3u} (10^{-4} erg s^{-1} cm^{-3})	0.442 $\pm$ 0.055	0.451 $\pm$ 0.055	0.455 $\pm$ 0.056	...
ℓ_{3v} (10^{-4} erg s^{-1} cm^{-3})	0.87 $\pm$ 0.12	0.89 $\pm$ 0.12	0.91 $\pm$ 0.12	...
ℓ_{3b} (10^{-4} erg s^{-1} cm^{-3})	0.94 $\pm$ 0.11	0.96 $\pm$ 0.11	0.97 $\pm$ 0.11	...
ℓ_{3y} (10^{-4} erg s^{-1} cm^{-3})	0.675 $\pm$ 0.078	0.685 $\pm$ 0.079	0.691 $\pm$ 0.079	...
C_u (erg s^{-1} cm^{-3})	1.3796 $\pm$ 0.0081	1.3946 $\pm$ 0.0081	1.4095 $\pm$ 0.0082	0.00075
C_v (erg s^{-1} cm^{-3})	0.9356 $\pm$ 0.0057	0.9482 $\pm$ 0.0058	0.9613 $\pm$ 0.0058	0.00064
C_b (erg s^{-1} cm^{-3})	0.6539 $\pm$ 0.0039	0.6615 $\pm$ 0.0039	0.6692 $\pm$ 0.0040	0.00038
C_y (erg s^{-1} cm^{-3})	0.4342 $\pm$ 0.0026	0.4382 $\pm$ 0.0026	0.4422 $\pm$ 0.0026	0.00020
C_u/C_v	1.475 $\pm$ 0.013	1.471 $\pm$ 0.012	1.466 $\pm$ 0.012	-0.00021
C_u/C_b	2.110 $\pm$ 0.018	2.108 $\pm$ 0.017	2.106 $\pm$ 0.018	-0.00008
C_u/C_y	3.177 $\pm$ 0.027	3.183 $\pm$ 0.026	3.187 $\pm$ 0.026	0.00025
C_v/C_b	1.431 $\pm$ 0.012	1.433 $\pm$ 0.012	1.437 $\pm$ 0.012	0.00015
C_v/C_y	2.155 $\pm$ 0.018	2.164 $\pm$ 0.018	2.174 $\pm$ 0.018	0.00048
C_b/C_y	1.506 $\pm$ 0.013	1.510 $\pm$ 0.017	1.513 $\pm$ 0.013	0.00018

Notes. RVs and $uvby$ light curves are from Southworth et al. (2005). The error in d is from van Leeuwen (2007), and not a solution error since d is a fixed parameter in this solution.

4.3. TY Pyxidis

TY Pyxidis is an RS CVn-type binary[11] of spectral-type G5V and orbit period 3.20 d. Although nearby with a good HIP distance of 56 pc, TY Pyx may not seem a good candidate for flux calibration due to erratic behavior, considering its surface brightness variations and consequent light curve irregularities caused by chromospheric and magnetic spot activity. It has a moderately large literature as a soft X-ray source (e.g., Franciosini et al. 2003; Ness et al. 2004; Güdel 2004) and as a radio source (e.g., Boboltz et al. 2003; Johnston et al. 2003). Since the number of well-observed EBs that are near enough

to be essentially extinction free is limited and circumstances are seldom perfect, the plan was to see if C_{band} measurement is robust enough to give reasonable results despite spots and other activity. Indeed, TY Pyx was more trouble than five ordinary systems, mainly due to its spotted surface, and iterations began from several starting points, some of which led to dead ends. One cannot expect to infer details of the spot distribution, so the spotted regions were represented by just one circular spot whose effective temperature supposedly approximates an average over the actual regions. Better light curve fits surely would be possible with two or more spotted areas, but our objective is estimation of calibration constants rather than a definitive general solution. Spot longitude and the dimensionless spot temperature factor were adjusted via least squares, while spot co-latitude (85°) and angular radius (20°) were not.

---

[11] RS CVn's are understood to have strong dynamo action, driven by convective motions in fast rotating envelopes. See Morgan & Eggleton (1979) for RS CVn evolution.
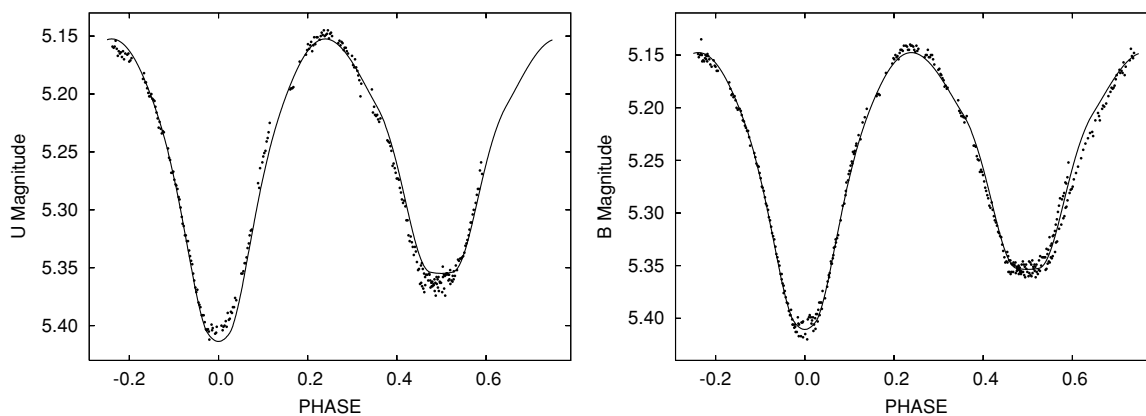
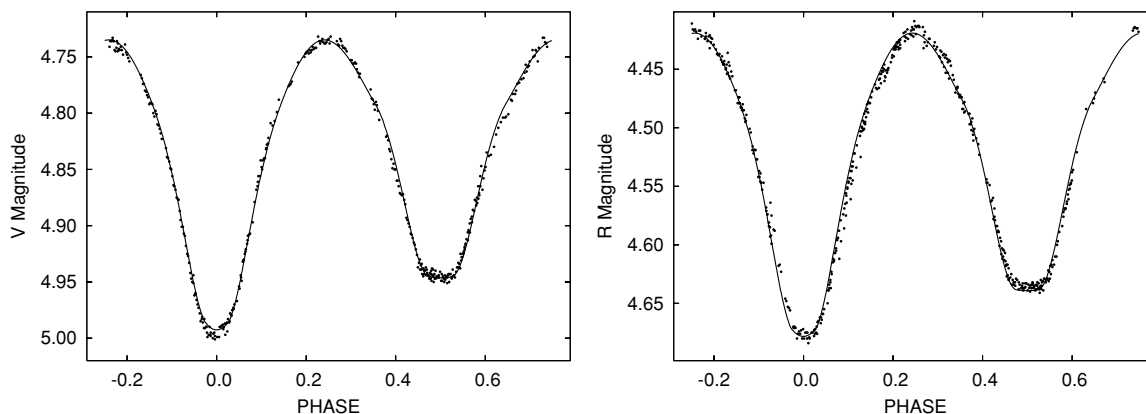**Figure 12.** ϵ CrA U (left) and B (right) curves for $1T-C_{band}$ solutions.

Figure 13. ϵ CrA V (left) and R (right) curves for $1T-C_{band}$ solutions.

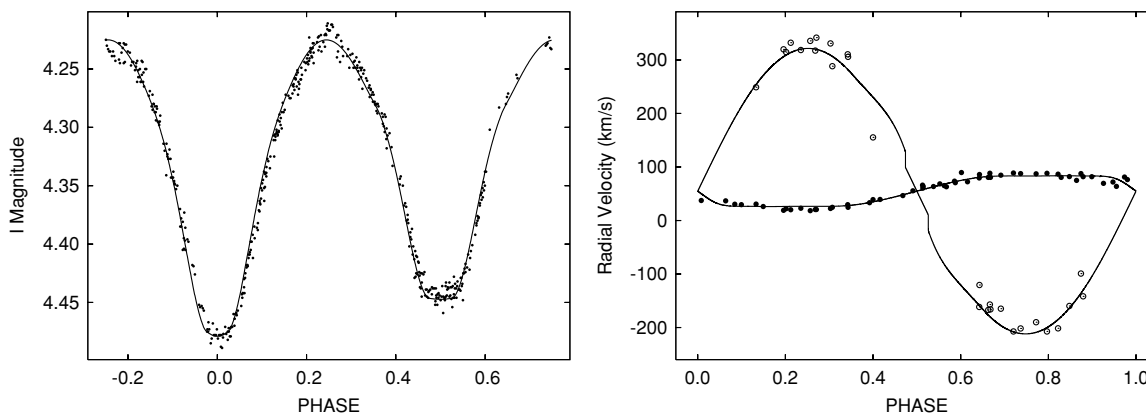**Figure 14.** ϵ CrA I (left) and RV (right) curves for $1T-C_{band}$ solutions.

Standard *uvby* magnitude data for the reference comparison star, HD 76483, are from Table 1 of Andersen et al. (1981a). Conversion of the differential photometry in Andersen et al. (1981b) to standard differential *uvby* is needed since HD 76483 is almost half a magnitude bluer than TY Pyx. Transformations in Grønbech et al. (1976) were applied, again following advice from J. V. Clausen. The components are nearly equal in mass, temperature, and luminosity. Star 2, as labeled by RV observers (Andersen & Popper 1975), is the one we call star 1, so the RV curves were interchanged, as also done in a solution by Andersen et al. (1981a). The Kreiner et al. (2001) timing diagrams show no indication of period change, but the ephemeris

was checked by including a reference epoch and period in the solution so as to make full use of timing information in the combined light and RV curves. The period thus derived is virtually identical to that by Andersen et al. (1981a) from eclipse timings. Metallicity [M/H] is close to zero (Nordström et al. 2004). Fixed input temperature T_1 was estimated via the scheme of Section 3.2. Iterations with multiple subsets were needed (Wilson & Biermann 1976) to achieve good convergence, although subset solutions were not needed for any of the other binaries. The observed and computed light curves are compared in Figure 11 to illustrate our limited success in dealing with the irregularities of this active binary.

4.4. V505 Persei

V505 Persei ($V \approx 6.86$ mag) is a detached, double-lined binary with two nearly identical F5V components in a 4.22 d orbit. Tomasella et al. (2008) obtained standard B, V light curves and RVs, and these data combined with the HIP (van Leeuwen 2007) distance of 61.6 ± 1.9 pc were used here for our C_B, C_V solution. The comparison star was HD 14444. T_1 (6512 K) and metallicity ([M/H] $= -0.12$) are from Tomasella et al. (2008), who determined these parameters from spectral analysis. Further information on the configuration is in Marschall et al. (1997), Munari et al. (2001), and Tomasella et al. (2008).

4.5. ϵ Coronae Australis

ϵ Coronae Australis is a well-known W UMa-type OC binary with a rather extreme mass ratio ($M_2/M_1 \approx 0.12$) and light curve asymmetries that indicate varying degrees of surface activity (magnetic spots) that affect the quality of fit. The HIP (van Leeuwen 2007) distance is 30.18 pc, with only a 1% error of 0.30 pc. The V magnitude is ≈ 4.8 mag and the spectral type is early F. Tapia (1969) gives an average $B - V$ of 0.412, which corresponds to a temperature of 6616 K according to the $T_{\rm eff} - (B - V) - $ [Fe/H] calibration Equation (1) of Alonso et al. (1996), assuming solar metallicity. For the same color, Table 15.7 in Cox (2004, p. 341) gives 6745 K. To find an estimate for T_1, we did not apply the method outlined in Section 3.2, but instead adopted $T_1 = 6700$ K and widely spaced bracket temperatures (see Table 8).

4.6. BG Indi

BG Indi is a sixth magnitude EB of spectral-type F3V in a 1.46 d orbit, as determined by Mathys et al. (1986), whose $uvby$ light curves were analyzed here. Additional differential magnitudes with respect to the comparison star HD 207964 were taken from Van Hamme & Manfroid (1988). The observations were transformed to standard $uvby$ magnitudes by addition of HD 207964 standard magnitudes (Hauck & Mermilliod 1998) to the differential magnitudes. A metallicity [M/H] of -0.30 equal to the [Fe/H] in Holmberg et al. (2007) was adopted. The input temperature T_1 was estimated to be 6450 K based on a color index $b - y = 0.291$ for the primary star, and applying the $(b - y)$ to $T_{\rm eff}$ calibration in Holmberg et al. (2007). The primary star color was inferred from the EB color at maximum light ($b - y = 0.316$), and a difference of 0.025 mag between the color of the two stars combined and that of the primary, estimated from a non-absolute light curve solution.

4.7. WW Aurigae

WW Aurigae ($V \approx 5.8$ mag) is a well detached, double-lined EB with a 2.53 days orbital period, consisting of two nearly equal metallic-line A-type stars. A fairly detailed analysis in Southworth et al. (2005) gives an overview of observational and solution papers. A DDE solution of the Southworth et al. (2005) $uvby$ curves with input of the Fabregat & Reig (1996) calibration constants is in Wilson & Van Hamme (2009). Our $C_{\rm band}$ solution is based on the same $uvby$ light and RV curves and the fixed HIP (van Leeuwen 2007) distance of 80.6 ± 2.3 pc, and a T_1 of 8000 K obtained with the method outlined in Section 4 of Southworth et al. Metallicity [M/H] is set at +0.50, in agreement with the high metal abundance of $Z = 0.06$ needed to reconcile absolute dimensions with evolution tracks, as argued by Southworth et al. (2005).

5. CONSISTENCY AND ERROR PROPAGATION

Band-to-band calibration ratios from EBs and single stars are independent of assumed distance while the individual $C_{\rm band}$'s from EB's are sensitive to assumed distance. We do not claim that our calibrations are more accurate than earlier ones, but only that they were derived differently. We do believe that our $C_{\rm band}$ ratios are improved in accuracy, as shown by their agreement for single stars, EBs, and the Sun. Some users of this work may want to condition previously published or otherwise independently determined $C_{\rm band}$'s to agree with ratios from this paper by making use of $C_{\rm band}$ averages in setting overall calibration levels. $C_{\rm band}$'s drawn from the literature might be acceptably accurate for $1T$ solutions while their ratios (which require *very* good accuracy when applied to $2T$ solutions) might produce somewhat wrong temperatures and therefore wrong distances. A reasonable strategy for distance applications is to adopt the new band-to-band $C_{\rm band}$ ratios while at least approximately preserving old $C_{\rm band}$ levels. For example, one could simply retain the calibration in one judiciously chosen band and revise the others according to the new ratios. However, exact preservation of both the ratio and mean value conditions is easy enough. First note that the geometric mean of $C_{\rm band}$'s is preferable to their arithmetic mean due to possible order of magnitude differences among bands. In the Strömgren systems, for example, let the "old" (i.e., from literature) calibration constants be C_u, C_v, C_b, C_y, and let the newly measured $C_{\rm band}^{\rm new}$ ratios be $\mathcal{R}_{uv}, \mathcal{R}_{vb}$, and $\mathcal{R}_{by}$. Then new calibrations that have the same geometric mean as the old ones and also agree with newly specified ratios are

$$
\begin{aligned}
C_y^{\rm new} &= \left((C_u C_v C_b C_y)/\left(\mathcal{R}_{uv} \mathcal{R}_{vb}^2 \mathcal{R}_{by}^3\right)\right)^{0.25}, \\
C_b^{\rm new} &= \mathcal{R}_{by} C_y^{\rm new}, \\
C_v^{\rm new} &= \mathcal{R}_{vb} C_b^{\rm new}, \\
C_u^{\rm new} &= \mathcal{R}_{uv} C_v^{\rm new}.
\end{aligned}
\tag{6}
$$

$C_{\rm band}$ dependence on star temperature was explored computationally via triplets of EB solutions that allow later interpolation or extrapolation among three T_1's. A similar strategy is not needed for adopted distance because of the exact dependence of $C_{\rm band}$ on d given by $C_{\rm band} = C_0 (d_0/d)^2$. Error estimates in $C_{\rm band}$ due to 1σ errors in T and in d are computed from $\frac{\partial C_{\rm band}}{\partial T} \cdot \sigma_T$ and $\frac{\partial C_{\rm band}}{\partial d} \cdot \sigma_d$, respectively. The total 1σ $C_{\rm band}$ errors in our EB calibration solution tables are the root-mean-square sums of these two terms since T and d come from mutually independent data.

Table 11 summarizes mean $C_{\rm band}$'s and $C_{\rm band}$ ratios for our seven calibration EBs. Means of $uvby$ calibration results in Table 12 were calculated in another way—among photometric bands for each of five EBs and for the single star data. Although these numbers are not applicable to absolute solutions, they give an impression of object to object consistency and point to a possible problem with WW Aur being a metallic-line star. The $C_{\rm band}$'s naturally jump around since they respond to the input HIP distance, with d errors producing d^2 errors in the $C_{\rm band}$'s. However, the ratios are unaffected by distance and should agree closely. Indeed, the single star and EB ratios easily agree to better than 1%, except for WW Aur which differs from the others by about 3%. An explanation for WW Aur in terms of interstellar extinction is possible but unlikely, as its distance is only ≈ 80 pc. A more likely reason is that WW Aur is well known as a strong metallic-line star, while the analysis program's Kurucz atmospheres are for normal stars. As we lack metallic-line SEDs at present, the best strategy may be to avoid use of the WW Aur results for distance estimation.

Table 11
Average EB $C_{\rm band}$'s and $C_{\rm band}$ Ratios

p	Number of EBs	Mean[a]	Mean[b]
C_u (erg s^{-1} cm^{-3})	5	1.335 ± 0.065	1.319 ± 0.082
C_v (erg s^{-1} cm^{-3})	5	0.946 ± 0.051	0.946 ± 0.066
C_b (erg s^{-1} cm^{-3})	5	0.653 ± 0.031	0.651 ± 0.041
C_y (erg s^{-1} cm^{-3})	5	0.418 ± 0.019	0.413 ± 0.024
C_u/C_v	5	1.405 ± 0.018	1.3889 ± 0.0098
C_u/C_b	5	2.044 ± 0.017	2.0269 ± 0.0015
C_u/C_y	5	3.198 ± 0.013	3.202 ± 0.016
C_v/C_b	5	1.453 ± 0.010	1.459 ± 0.011
C_v/C_y	5	2.270 ± 0.036	2.305 ± 0.025
C_b/C_y	5	1.563 ± 0.016	1.5800 ± 0.0073
C_U (erg s^{-1} cm^{-3})	1	0.4950	...
C_B (erg s^{-1} cm^{-3})	2	0.614 ± 0.045	...
C_V (erg s^{-1} cm^{-3})	2	0.374 ± 0.017	...
C_R (erg s^{-1} cm^{-3})	1	0.2011	...
C_I (erg s^{-1} cm^{-3})	1	0.1007	...
C_U/C_B	1	0.704	...
C_U/C_V	1	1.228	...
C_U/C_R	1	2.462	...
C_U/C_I	1	4.914	...
C_B/C_V	2	1.652 ± 0.052	...
C_B/C_R	1	3.497	...
C_B/C_I	1	6.98	...
C_V/C_R	1	2.005	...
C_V/C_I	1	4.003	...
C_R/C_I	1	1.996	...

Notes.
[a] Weighted mean and standard error of the mean, with weights inversely proportional to individual mean errors in Tables 4, 5, 6, 9, and 10.
[b] Same as Column 4 for the four EBs with WW Aur excluded (see Section 5).

Table 12
Comparison of Mean *uvby* Calibrations and Calibration Ratios

Source	$C_{\rm uvby}$ (erg s^{-1} cm^{-3})	$C_{\rm uvby}$ Ratio
Single stars	0.6837	2.0644
BG Ind	0.6002	2.0792
WW Aur	0.7868	2.1450
TZ Men	0.7454	2.0770
TY Pyx	0.6775	2.0957
V1130 Tau	0.8426	2.0796

Notes. The $C_{\rm uvby}$'s are geometric means of C_u, C_v, C_b, and C_y. The $C_{\rm uvby}$ ratios are geometric means of C_u/C_v, C_u/C_b, and C_u/C_y.

5.1. Tests of New $C_{\rm band}$ Ratios: T_1, T_2, d Solutions for V505 Per and WZ Oph

With $C_{\rm band}$ ratios from 462 single stars, the Sun, and seven EBs in hand, one can check whether $2T$ EB solutions by the DDE algorithm now give temperatures in agreement with spectroscopic estimates within realistic uncertainties, as has *not* been the case (Wilson 2008; Wilson & Van Hamme 2009) with previously available $C_{\rm band}$ ratios that gave systematically high $2T$ temperatures, typically by several hundred Kelvin. Proper statistical results on this issue naturally await future work by many persons, but here we make a beginning. Difficulties with spectroscopic temperatures are briefly discussed in Section 1.2. As the objective of our emphasis on $C_{\rm band}$ ratios is to have a realistic alternative ($2T$ solutions) to spectroscopic temperatures, we checked DDE T's against spectroscopic T's for the well-observed and uncomplicated main-sequence EBs V505 Persei and WZ Ophiuchi. BV calibration constants for both binaries,

Table 13
EB Two-temperature and Distance Solutions from New Calibrations

Parameter	V505 Per	WZ Oph
T_0 (HJD)	$2451587.30640 \pm 0.00015$	2450535.783310
P (d)	4.2220169 ± 0.0000022	4.183506810
$a/R_\odot$	15.049 ± 0.022	14.715 ± 0.038
V_γ (km s^{-1})	0.23 ± 0.09	-28.34 ± 0.28
i (deg)	87.872 ± 0.018	89.196 ± 0.022
T_1 (K)	6743 ± 4	6136 ± 36
T_2 (K)	6691 ± 4	6121 ± 36
Ω_1	12.234 ± 0.090	11.404 ± 0.023
Ω_2	12.730 ± 0.100	11.363 ± 0.049
$q = M_2/M_1$	0.9861 ± 0.0028	0.9979 ± 0.0046
d (pc)	66.00 ± 0.23	166.2 ± 2.3
$d_{\rm HIP}$ (pc)	61.6 ± 1.9	151 ± 29
ℓ_{3B}	...	3.25 ± 0.29
ℓ_{3V}	...	1.45 ± 0.18
ℓ_{3R_C}	...	2.14 ± 0.18
ℓ_{3I_C}	...	2.15 ± 0.13
ℓ_{3u}	...	1.61 ± 0.13
ℓ_{3v}	...	1.50 ± 0.16
ℓ_{3b}	...	0.50 ± 0.19
ℓ_{3y}	...	0.82 ± 0.17
$\ell_3/\ell_{{\rm total}\,B}$	...	0.0366 ± 0.0033
$\ell_3/\ell_{{\rm total}\,V}$	...	0.0171 ± 0.0021
$\ell_3/\ell_{{\rm total}\,R_C}$	...	0.0304 ± 0.0026
$\ell_3/\ell_{{\rm total}\,I_C}$	...	0.0424 ± 0.0026
$\ell_3/\ell_{{\rm total}\,u}$	...	0.0306 ± 0.0025
$\ell_3/\ell_{{\rm total}\,v}$	...	0.0175 ± 0.0019
$\ell_3/\ell_{{\rm total}\,b}$	...	0.0052 ± 0.0020
$\ell_3/\ell_{{\rm total}\,y}$	...	0.0096 ± 0.0020

Notes. The ℓ_3 unit is 10^{-6} erg s^{-1} cm^{-3}, with $\ell_{\rm total}$ meaning total system light at phase 0.25. The standard errors on fractional third light ($\ell_3/\ell_{\rm total}$) assume negligible errors in $\ell_{\rm total}$.

as well as *uvby* constants for WZ Oph, are from Table 1. WZ Oph also needed calibrations for Cousins R_C and I_C, which are from Bessell (1979, after conversion of units).

V505 Per—one of our "calibration stars"—is used here in a $2T$ temperature–distance solution to check agreement with spectral temperatures. The applied $C_{\rm band}$'s are not from the calibration solution but from our single star means, so the overall process is not circular. Our distance solutions were in two bands (B and V), in accord with the T–d theorem (Wilson 2007, 2008). Solution parameters are in Table 13. The resulting T_1 of 6743 K is 230 K higher (about two spectral subclasses) than in Tomasella et al. (2008), although only 93 K higher (less than a subclass) than indicated by its F5 spectral type according to Table 15.7 of Cox (2004, p. 341). Interpolation in the Cox table gives a spectral type of about F4.5 for a straight average of our T_1 and T_2, so the new $C_{\rm band}$ ratios may or may not give essential agreement with spectroscopic temperature, depending on the spectroscopic result to which they are compared. Further exploration of V505 Per temperatures seems needed. The DDE distance is 66.00 ± 0.23 pc, which compares to the revised HIP distance of 61.6 ± 2.2 pc by van Leeuwen (2007).[12] Parallaxes from the Gaia mission should settle this marginally significant (2σ) distance issue.

WZ Oph was observed on 28 nights in 2008 May and June with the 0.4 m Schmidt–Cassegrain telescope at Sonoita Research Observatory (SRO) in Sonoita, AZ. A Santa Barbara

---

[12] Perhaps worth noting is that the original HIP distance by Perryman et al. (1997) is 66.6 ± 3.9 pc, in agreement with DDE.
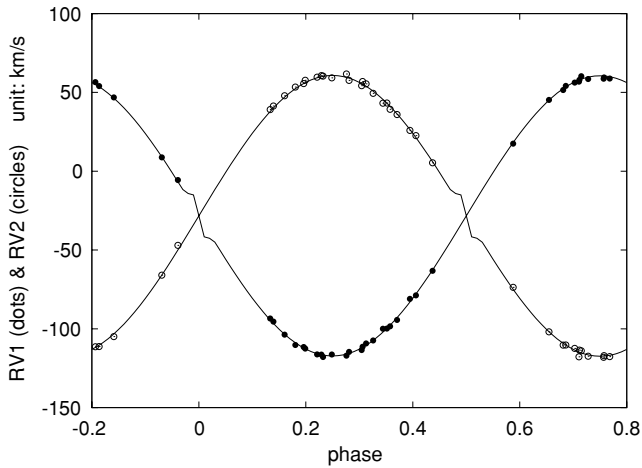
Figure 15. WZ Oph observed (dots) and model (lines) RV curves for the RV + eight-band distance solution.

Table 14
New WZ Oph Photometric Observations

HJD	B (mag)	V (mag)	R_C (mag)	I_C (mag)
2454641.6593	9.592	9.070	8.711	8.450
2454641.6603	9.586	9.077	8.765	8.450
2454641.6781	9.617	9.092	8.759	8.438

(This table is available in its entirety in a machine-readable form in the online journal. A portion is shown here for guidance regarding its form and content.)

Instrument Group STL-1001XE CCD camera with Johnson B and V and Cousins R_C and I_C filters took 751 B, V, R_C, I_C image sets that were bias/dark subtracted and flat-fielded with the Image Reduction and Analysis Facility (IRAF) of the National Optical Astronomy Observatories. Differential photometry was then performed with TYC 977-116-1 as the comparison (C) star and TYC 976-1177-1 as a check (K) star. The C − K differential magnitudes had a standard deviation of about 0.01 mag over the entire observing interval. The Tycho comparison star observations yielded $B - V = 0.55 \pm 0.04$ while SRO observations over 13 photometric nights, with Landolt standards, yielded $B - V = 0.54 \pm 0.02$. Observations of WZ Oph from SRO on those 13 nights yielded $B - V = 0.54 \pm 0.05$. The identical colors of the comparison star and WZ Oph, along with the lack of variability in the comparison star, confirm its suitability for the differential photometry. The differential magnitudes were then transformed to the standard B, V, R_C, and I_C systems with the transformation coefficients for the SRO instrumentation. Estimated standard deviations are 0.025 mag in B, 0.012 mag in V, 0.017 mag in R_C, and 0.018 mag in I_C. Because of the good color match and the proximity of the comparison star to WZ Oph, no corrections for differential atmospheric extinction were necessary.

A comprehensive discussion of WZ Oph with a full traditional light/RV analysis is in Clausen et al. (2008a). Here, we ran their

observations through the DDE algorithm to check whether our new $C_{\rm band}$ ratios lead to temperatures that agree with spectral information in the literature. WZ Oph is well detached with orbit period 4.18 d and main-sequence components of nearly equal mass and early G spectral type. It poses an interesting situation with regard to the T–d theorem's advice that two bands (not one, not three or more) should be entered into a $2T$ absolute solution. The interesting point is that we have the unusual number of eight bands (u, v, b, y, B, V, R_C, and I_C) and would like to utilize all, but solutions of the 28 two-band combinations and subsequent inter-comparisons would be tedious. However, the sole reason not to process three or more light curves together is to avoid the non-Gaussian residuals that go with overall misfits that are likely to arise from errors in the calibrative data. Because of the possibility that there may be no misfits (and curiosity about how large they might be), the eight bands were entered together, with the unexpected result that all bands were matched rather well—there was no obvious non-Gaussian problem. Accordingly, the Strömgren u, v, b, y—Johnson B, V—Cousins R_C, I_C solution, with RVs from Clausen et al. (2008a), is the one reported in Table 13, with the RVs shown in Figure 15 and the light curves in Figure 16. The $uvby$ curves are from Clausen et al. (2008b) and the B, V, R_C, and I_C curves from Table 14. The temperatures from our DDE solution, $T_1 = 6136 \pm 36$ K and $T_2 = 6121 \pm 36$ K, are the same as found by Clausen et al. (2008a; $T_1 = 6165 \pm 100$ K, $T_2 = 6165 \pm 100$ K), well within the 1σ uncertainties, after the extensive processing of spectra and light curves by Clausen et al. (2008a). Note that our T_1 and T_2 standard errors are much larger than for V505 Per. The reason is that the WZ Oph solution includes third light, which is correlated with T_1 and T_2. For WZ Oph, at least, the $2T$ test results are consistent with $C_{\rm band}$ ratios now being accurate. The DDE distance is 166.2 ± 2.3 pc, in agreement with 151 ± 29 pc from parallax (van Leeuwen 2007).
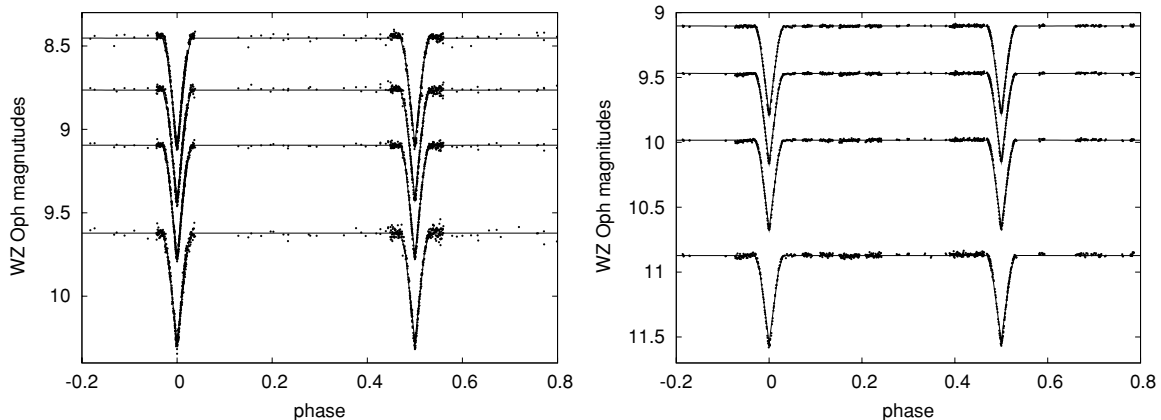

Figure 16. WZ Oph observed (dots) and model (lines) light curves for the eight-band distance solution (left panel, bottom to top: B, V, R_C, and I_C; right panel, bottom to top: u, v, b, and y). Note that agreement is good not only in form, but also in absolute level for all bands, which can happen only if the input calibration ratios are accurate.

6. FINAL COMMENTS

To underscore the aims, usefulness, and some active problems of C_{band} measurement by the ways of this paper, we emphasize several key points.

1. Simulations show that correct recovery of T_1 and T_2 in two-band DDE solutions hinges on the two C_{band}'s being in the correct ratio. As intuition predicts, a pair of C_{band}'s that are individually wrong but have the correct ratio lead to accurate T's, and a distance that is off only by a $C_{band}^{-1/2}$ factor, in adherence to the inverse square law of flux dilution. So a C_{band} error of 4% leads to a distance error of only 2% in a one-band solution, and that will also be the case in a two-band or multi-band solution if the ratio of C_{band}'s is correct. Of course any deficiencies in model atmospheres and in transformations to standard photometric systems also contribute to overall distance errors.

2. The relevant response functions for EB distances by the DDE algorithm are those applied within DDE. The frequently cited *uvby* instrumental functions by Crawford & Barnes (1970) and Matsushima (1969) are described by those authors as filter transmission functions so it is important to know that the *uvby* functions utilized by DDE are the Crawford & Barnes (1970) filter transmissions multiplied by photomultiplier response and by Earth atmosphere transmission and two aluminum reflections (Allen 1973, p. 108). The assumed photomultiplier response is that of a nominal RCA 1P21 phototube, which is the type used for most or all of the original *uvby* standard star observations.

3. The (inverted) DDE process finds individual C_{band}'s that can have relatively large uncertainty for a given EB because measured C_{band} scales (inversely) with the *square* of the adopted distance. However, results can be averaged and should improve as C_{band}'s are estimated for ever more binaries. Furthermore, individual C_{band}'s are not needed to great accuracy because they are applied to find d from C_{band} rather than C_{band} from d, with $d \propto 1/\sqrt{C_{band}}$.

4. The future is bright for improved individual C_{band} measurement for EBs because the coming Gaia mission[13] will determine parallaxes of order 100 times more accurate than those of the *Hipparcos* catalog. With C_{band} ratios very solidly determined (for which this paper is only a beginning), an accurate absolute calibration for any one band sets the calibrations for many bands.

5. Little has been published on accurate magnitude to physical flux calibrations for other than the Johnson, Cousins, Strömgren, and Two Micron All Sky Survey bands, so calibrations and calibration ratios are needed for the neglected bands. Distances from infrared bands are particularly important because of their relative freedom from interstellar extinction.

6. Convergence is remarkably strong in all of our C_{band} and C_{band} ratio solutions for EBs, often attaining essentially final results in one or two iterations. Negligibly, different results are reached from varied starting points.

7. Integration of empirical SEDs over response functions as in Bessell (1979), Fabregat & Reig (1996), and others remains an accurate way to evaluate individual C_{band}'s. They can be adjusted to have given ratios (such as those of this paper) while retaining their (geometric) means by Equations (6).

8. Although a C_{band} measured for an individual single star (Section 2.2) may be inaccurate due to radius uncertainty, the number of potential targets is large, so averaged results can be accurate. For example, a mean C_{band} based on 400 stars has its standard error reduced by a factor of 20.

REFERENCES

Allen, C. W. 1973, Astrophysical Quantities (3rd ed.; London: Athlone)
Alonso, A., Arribas, S., & Martínez-Roger, C. 1996, A&A, 313, 873
Andersen, J., Clausen, J. V., & Nordström, B. 1987, A&A, 175, 60
Andersen, J., Clausen, J. V., Nordström, B., & Reipurth, B. 1981a, A&A, 101, 7
Andersen, J., Clausen, J. V., Nordström, B., & Reipurth, B. 1981b, A&AS, 43, 141
Andersen, J., & Popper, D. M. 1975, A&A, 39, 131
Ažusienis, A., & Straižys, V. 1969, SvA, 13, 316
Bakiş, V., et al. 2010, New Astron., 15, 1
Barnes, T. G. 2009, in AIP Conf. Proc. 1170, Stellar Pulsation: Challenges for Theory and Observation, ed. J. A. Guzik & P. A. Bradley (New York: Springer), 3
Barnes, T. G., Storm, J., Jefferys, W. H., Gieren, W. P., & Fouque, P. 2005, ApJ, 631, 572
Bessell, M. S. 1979, PASP, 91, 589
Bessell, M. S. 1983, PASP, 95, 480
Boboltz, D. A., Fey, A. L., Johnston, K. J., Claussen, M. J., de Vegt, C., Zacharias, N., & Gaume, R. A. 2003, AJ, 126, 484
Bonanos, A. Z., et al. 2006, ApJ, 652, 313
Buser, R. 1978, A&A, 62, 411
Casagrande, L., Flynn, C., & Bessell, M. 2008, MNRAS, 389, 585
Casagrande, L., Portinari, L., & Flynn, C. 2006, MNRAS, 373, 13
Casagrande, L., Ramirez, I., Melendez, J., Bessell, M., & Asplund, M. 2010, A&A, 512, A54
Clausen, J. V., Olsen, E. H., Helt, B. E., & Claret, A. 2010, A&A, 510, A91
Clausen, J. V., Storm, J., Larsen, S. S., & Gimenez, A. 2003, A&A, 402, 509
Clausen, J. V., Torres, G., Bruntt, H., Andersen, J., Nordström, B., Stefanik, R. P., Latham, D. W., & Southworth, J. 2008a, A&A, 487, 1095
Clausen, J. V., Vaz, L. P. R., Garcia, J. M., Gimenez, A., Helt, B. E., Olsen, E. H., & Andersen, J. 2008b, A&A, 487, 1081
Cohen, M., Wheaton, W. A., & Megeath, S. T. 2003, AJ, 126, 1090
Cox, A. N. 2004, Allen's Astrophysical Quantities (4th ed.; New York: Springer)
Crawford, D. L., & Barnes, J. V. 1970, AJ, 75, 978
Davis, J., Jacob, A. P., Robertson, J. G., Ireland, M. J., North, J. R., Tango, W. J., & Tuthill, P. G. 2009, MNRAS, 394, 1620
Di Benedetto, G. P. 2005, MNRAS, 357, 174
Di Benedetto, G. P. 2008, MNRAS, 390, 1762
Eisner, J. A., et al. 2007, ApJ, 654, L77
Fabregat, J., & Reig, P. 1996, PASP, 108, 90
Fouque, P., et al. 2007, A&A, 476, 73
Franciosini, E., Pallavicini, R., & Tagliaferri, G. 2003, A&A, 399, 279
Gieren, W., Storm, J., Barnes, T. G., Fouque, P., Pietrzynski, G., & Kienzle, F. 2005, ApJ, 627, 224
Goecking, K. D., & Duerbeck, H. W. 1993, A&A, 278, 463
Gray, R. O. 1998, AJ, 116, 482
Grønbech, B., Andersen, J., Clausen, J. V., Nordström, B., & Reipurth, B. 1987, A&AS, 68, 331
Grønbech, B., Olsen, E. H., & Strömgren, B. 1976, A&AS, 26, 155
Güdel, M. 2004, A&AR, 12, 71
Guinan, E. F., et al. 1998, ApJ, 509, L21

---

[13] See http://sci.esa.int/science-e/www/area/index.cfm?fareaid=26.

Harries, T. J., Hilditch, R. W., & Howarth, I. D. 2003, MNRAS, 339, 157
Hauck, B., & Mermilliod, M. 1998, A&AS, 129, 431
Heber, U., Hunger, K., Jonas, G., & Kudritski, R. P. 1984, A&A, 130, 119
Helt, B. E., et al. 1991, A&AS, 89, 399
Hernández, C. A. 1972, AJ, 77, 152
Holmberg, J., Nordström, B., & Andersen, J. 2007, A&A, 475, 519
Johnson, H. L. 1965a, Commun. Lunar Planet. Lab., 3, 73
Johnson, H. L. 1965b, ApJ, 141, 923
Johnson, H. L. 1966, ARA&A, 4, 193
Johnston, K. J., de Vegt, C., & Gaume, R. 2003, AJ, 125, 3252
Kervella, P., Bersier, D., Mourard, D., Nardetto, N., Fouque, P., & Coude du
    Foresto, V. 2004, A&A, 428, 587
Kreiner, J. M., Kim, C., & Nha, I. 2001, An Atlas of $O - C$ Diagrams of Eclipsing
    Binary Stars (Krakow: Wydawnictwo Naukowe Akademii Pedagogicznej)
Kruszewski, A., & Semeniuk, I. 1999, Acta Astron., 49, 561
Kurucz, R. 1993, in IAU Symp. 151, Light Curve Modeling of Eclipsing Binary
    Stars, ed. E. F. Milone (New York: Springer), 93
Landolt, A. U. 1992, AJ, 104, 340
Landolt, A. U. 2007, AJ, 133, 2502
Landolt, A. U. 2009, AJ, 137, 4186
Lanz, T. 1986, A&AS, 65, 195
Macri, L. M. 2005, arXiv:astro-ph/0507648
Marschall, L. A., Stefanik, R. P., Lacy, C. H., Torres, G., Williams, D. B., &
    Agerer, F. 1997, AJ, 114, 793
Mathys, G., Manfroid, J., & Renson, P. 1986, A&AS, 63, 403
Matsushima, S. 1969, ApJ, 158, 1137
Mermilliod, J. C. 1997, VizieR Online Data Catalog, 2168
Morgan, J. G., & Eggleton, P. P. 1979, MNRAS, 187, 661
Munari, U., et al. 2001, A&A, 378, 477
Ness, J. U., Güdel, M., Schmitt, J. H. M. M., Audard, M., & Telleschi, A.
    2004, A&A, 427, 667
Nidever, D. L., Marcy, G. W., Butler, R. P., Fischer, D. A., & Vogt, S. S.
    2002, ApJS, 141, 503
Nordström, B., et al. 2004, A&A, 418, 989
Ostrov, P. G., & Lapasset, E. 2003, MNRAS, 338, 141
Paczynski, B. 1997, in The Extragalactic Distance Scale, ed. M. Livio (Cam-
    bridge: Cambridge Univ. Press), 273

Pasinetti Fracassini, L. E., Pastori, L., Covino, S., & Pozzi, A. 2001, A&A, 367,
    521
Perryman, M. A., et al. 1997, A&A, 323, L49
Pourbaix, D., et al. 2009, VizieR Online Data Catalog, 1, 2020
Russell, H. N. 1948, Harvard Obs. Monogr., 7, 249
Southworth, J., Smalley, B., Maxted, P. F. L., Claret, A., & Etzel, P. B.
    2005, MNRAS, 363, 529
Storm, J., Gieren, W. P., Fouque, P., Barnes, T. G., & Gomez, M. 2005, A&A,
    440, 487
Tapia, S. 1969, AJ, 74, 533
Tapia, S., Johnson, H. L., & Crawford, D. L. 1973, in IAU Symp. 54, Problems
    of Calibration of Absolute Magnitudes and Temperatures of Stars, ed. B.
    Hauck & B. E. Westerlund (Dordrecht: Reidel), 163
Tomasella, L., Munari, U., Siviero, A., Cassini, S., Dallaporta, S., Zwitter, T.,
    & Sordo, R. 2008, A&A, 480, 465
Valenti, J. A., & Fischer, D. A. 2005, ApJS, 159, 141
Van Hamme, W. 1993, AJ, 106, 2096
Van Hamme, W., & Manfroid, J. 1988, A&AS, 74, 247
Van Hamme, W., & Wilson, R. E. 2003, in ASP Conf. Ser. 298, Gaia
    Spectroscopy, Science and Technology, ed. U. Munari (San Francisco, CA:
    ASP), 323
Van Hamme, W., & Wilson, R. E. 2007, ApJ, 661, 1129
van Leeuwen, F. 2007, A&A, 474, 653
Vilardell, F., Ribas, I., Jordi, C., Fitzpatrick, E. L., & Guinan, E. F. 2010, A&A,
    509, A70
Welch, D. L. 1994, AJ, 108, 1421
Wilson, R. E. 1979, ApJ, 234, 1054
Wilson, R. E. 1990, ApJ, 356, 613
Wilson, R. E. 2005, Ap&SS, 296, 197
Wilson, R. E. 2007, in ASP Conf. Ser. 362, The Seventh Pacific Rim Conference
    on Stellar Astrophysics, ed. Y. W. Kang et al. (San Francisco, CA: ASP), 3
Wilson, R. E. 2008, ApJ, 672, 575
Wilson, R. E., & Biermann, P. 1976, A&A, 48, 349
Wilson, R. E., & Devinney, E. J. 1971, ApJ, 166, 605
Wilson, R. E., & Van Hamme, W. 2009, ApJ, 699, 118
Wilson, R. E., & Van Hamme, W. 2010, in ASP Conf. Ser. 435, Binaries—Key
    to Comprehension of the Universe, ed. A. Prsa (San Francisco, CA: ASP),
    45